https://doi.org/10.5194/egusphere-2024-1440
Preprint. Discussion started: 23 May 2024


# Observations of methane net sinks in the Arctic tundra

Antonio Donateo[1*], Daniela Famulari[2], Donato Giovannelli[3,4,5,6,7], Arturo Mariani[8], Mauro Mazzola[9], Stefano Decesari[10], Gianluca Pappaccogli[1,11]

[1] National Research Council of Italy, Institute of Atmospheric Sciences and Climate (CNR-ISAC), 73100, Lecce - Italy
[2] National Research Council of Italy, Institute of BioEconomy (CNR-IBE), 40129, Bologna – Italy
[3] University of Naples "Federico II", Department of Biology, 80126 Napoli - Italy
[4] Institute for Marine Biological and Biotechnological Resources, National Research Council of Italy (CNR-IRBIM), Ancona, Italy
[5] Woods Hole Oceanographic Institution, Marine Chemistry and Geochemistry Department, MA, USA
[6] Tokyo Institute of Technology, Earth-Life Science Institute, ELSI, Tokyo, Japan
[7] Rutgers University, Department of Marine and Coastal Science, New Brunswick, NJ, USA
[8] GeoSystems s.r.l., 50122, Firenze - Italy
[9] National Research Council of Italy, Institute of Polar Sciences (CNR-ISP), 40129, Bologna
[10] National Research Council of Italy, Institute of Atmospheric Sciences and Climate (CNR-ISAC), 40129, Bologna
[11] JRC - ENI-CNR Aldo Pontremoli, 73100, Lecce – Italy

*Correspondence to*: Antonio Donateo (a.donateo@isac.cnr.it)

**Abstract.** This study focuses on direct measurements of $CO_2$ and $CH_4$ turbulent eddy covariance fluxes in tundra ecosystems in the Svalbard Islands over a two-year period. Our results reveal dynamic interactions between climatic conditions and ecosystem activities such as photosynthesis and microbial activity. During summer, pronounced carbon uptake fluxes indicate increased photosynthesis and microbial methane consumption, while during the freezing seasons very little exchange was recorded, signifying reduced activity. The observed net summertime methane uptake is correlated with the activation and aeration of soil microorganisms, and it declines in winter due to the presence of snow cover and because of the low soil temperatures, but then rebounds during the melting period. $CH_4$ fluxes are not significantly correlated with temperature, but are instead associated with wind velocity, suggesting that electron acceptor limitation may be stimulating methanotrophic communities. High temperature anomalies increase $CO_2$ emissions, which may have the effect of limiting summer productivity and carbon sequestration. Positive methane fluxes (emissions) were observed during warm anomalies in winter. These findings emphasise the necessity of comprehending the dynamics of greenhouse gases in tundra ecosystems in order to mitigate climate change. Further research is required to elucidate the sources and sinks of greenhouse gases in dry tundra ecosystems.

https://doi.org/10.5194/egusphere-2024-1440
Preprint. Discussion started: 23 May 2024


## 1 Introduction

The Arctic region is experiencing rapid climate change in response to the increase in greenhouse gases (GHGs), aerosols, and other climate drivers, which leads to alterations in the biogeochemical cycles of carbon and other GHGs (Stjern et al., 2019). This phenomenon is known as Arctic amplification (Serreze and Barry, 2011; Schmale et al., 2021). Arctic warming is essentially driven by changes in anthropogenic GHGs and short-lived climate forcers, such as methane, tropospheric ozone, and aerosols, affect the Arctic climate (Howarth et al., 2011; Arnold et al., 2016; Law et al., 2014; Sand et al., 2015). Methane ($CH_4$) and carbon dioxide ($CO_2$) are two of the most significant greenhouse gases that contribute to climate change, and their fluxes in the Arctic have been of great interest to researchers in recent years. Methane is a potent greenhouse gas (global average ~1.8 ppm) with a global warming potential that is about 28 times greater than that of carbon dioxide over a 100-year timescale (Myhre et al., 2013). Thus, quantifying the natural sources and sinks of $CH_4$ is critical for understanding and predicting how climate change will impact its cycling in northern environments. Lara et al. (2018) estimated that the Arctic tundra alone could become a net source of carbon by the mid- to late-21st century, due to the thawing of permafrost. Dean et al. (2018, 2020) found that Arctic lakes released significantly more methane owing to warming temperatures, with the potential to offset any carbon uptake from other Arctic ecosystems. Arctic amplification has also been found to decrease the absorption of GHGs, particularly $CO_2$, in the Arctic region (Zona et al., 2022). This is because reduced soil moisture during the peak summer can limit plant productivity, thus reducing the ability of these ecosystems to capture carbon during that season.

In the Arctic, methane and carbon dioxide fluxes are influenced by a variety of environmental factors, including permafrost thawing, changes in vegetation cover, and changes in water levels. As permafrost thaws, the organic matter it contains becomes more accessible for microbial decomposition, leading to increased methane, carbon dioxide and other greenhouse gas emissions due to microbial mediated degradation activity (Knoblauch et al., 2018; Kleber et al., 2023). Notably, the primary driver of this net $CO_2$ uptake was vegetation; however, during the winter months, the soil acted as a $CO_2$ source. Tundra ecosystems are also known to produce methane ($CH_4$) as the final product of microbial metabolism through an anaerobic biotic process known as methanogenesis (Cicerone and Oremland, 1988). Methanogenesis is common in a variety of ecosystems, and it is generally found in strictly anoxic environments and in the deeper soil and sedimentary layers coupled to the final steps of the decay of organic matter (Hodson et al., 2019). Methane uptake occurs in the atmosphere through chemical and/or photochemical oxidation, or biologically in soil and in water, through methane-oxidising bacteria and archaea (hereafter methanotrophy) that use methane as a source of energy and carbon (Serrano-Silva et al., 2014). The oxidation of methane by microorganisms can happen in two general forms, aerobically, coupled to the reduction of oxygen in oxic environments, and anaerobically in anoxic ecosystems, a process known as anaerobic methane oxidation, coupling methane to electron acceptors such as sulphate, nitrate, iron (III) and manganese (IV) either by single microorganisms or microbial consortia (Guerrero-Cruz et al., 2021).

https://doi.org/10.5194/egusphere-2024-1440
Preprint. Discussion started: 23 May 2024


Historically, most studies on methane emissions in the Arctic have focused on wetlands and wet tundra ecosystems (Tan et al., 2016), because they provide the most consistent data to evaluate total natural methane emissions in high latitudes (AMAP, 2021). The projections of future emissions in the Arctic are complicated by the multiple effects of changes in temperature and precipitation regimes in the individual ecosystems: while a wetter, warmer climate is generally associated with an increase in natural methane emissions, drier summers can lead to increased respiration rates in soils and reduced releases of methane. Wetland and organic carbon-rich ecosystems, however, cover a relatively small area in the Arctic region when compared with well-aerated mineral soils (Hugelius et al., 2014; Jørgensen et al., 2015; Emmerton et al., 2016). Relatively dry, well drained upland terrains and generally dry tundra ecosystems can act as significant methane sinks rather than sources over large geographical sectors of the Arctic (Emmerton et al., 2014; Jørgensen et al., 2015; D'Imperio et al., 2017; Oh et al., 2020). Due to the uncertainties in regional climate projections and in the carbon cycle response, it remains unclear whether the Arctic will play a larger role in the global $CH_4$ budget with future climate change (AMAP, 2021). Several studies have investigated the sources and sinks of methane in dry tundra ecosystems, especially by means of chamber measurement systems. Lindroth et al. (2022) measured the methane emissions from different types of tundra in Svalbard. The study revealed that wet tundra with waterlogged soil was a notable methane emission source, while the vegetation in the tundra served as a carbon dioxide sink. Mastepanov et al. (2008) investigated $CH_4$ fluxes in a dry tundra ecosystem in north-eastern Siberia, finding that the ecosystem was a small net source of $CH_4$, with the highest emissions occurring during the summer. This study also found that $CH_4$ emissions were strongly influenced by soil moisture and temperature, with wetter and warmer soils leading to higher emissions. Wagner et al. (2019), with their measurements on the southern shore of Melville Island in the Canadian Arctic Archipelago, demonstrate that net $CH_4$ uptake may be largely underestimated across the Arctic due to sampling bias towards wetlands. Combining in situ flux data with laboratory investigations and a machine learning approach, Voigt et al. (2023) find biotic drivers to be highly important in absorption of atmospheric $CH_4$ on well-drained Arctic soils. These work conclusions imply that soil drying, and enhanced nutrient supply will promote $CH_4$ uptake by Arctic soils, providing a negative feedback to global climate change. Juncher Jørgensen et al. (2015) combining chamber in situ measurements with satellite remote sensing observations, conclude that the ice-free area of northeast Greenland acts as a net sink of atmospheric methane, and suggest that this sink will probably be enhanced under future warmer climatic conditions. Further, research on dry tundra ecosystems has focused primarily on $CO_2$ and $CH_4$ emissions during snow-free periods. However, $CH_4$ emissions from tundra ecosystems were not limited to the growing season. Bao et al. (2021) found that high $CH_4$ efflux and emission pulses can occur during shoulder seasons, such as autumn and spring thaw. This study suggests that shoulder season $CH_4$ emissions should be considered when assessing the total annual $CH_4$ emissions from tundra ecosystems. However, there is a noticeable lack of studies investigating these emissions across various seasonal phases, with a specific focus on how thermal anomaly patterns affect GHGs fluxes (Bao et al., 2021, Ishizawa et al., 2023). This knowledge gap holds significant importance in our efforts to understand the equilibrium between $CO_2$ and $CH_4$ in dry tundra environments, particularly given the increasing frequency and intensity of extreme events. Long-term studies covering multiple seasonal cycles have been limited owing to logistical challenges, especially during cold,

https://doi.org/10.5194/egusphere-2024-1440
Preprint. Discussion started: 23 May 2024


snow-covered seasons (Arndt et al., 2019; Mastepanov et al., 2008, 2013; Pirk et al., 2015, 2016; Taylor et al., 2018; Zona et al., 2016; Bao et al., 2021). It is important to quantify the amount of gases released into the atmosphere at regional scale (Treat et al., 2024), as well as the processes that control their release, to accurately model future climate scenarios.

This work aims to quantify the exchange fluxes of carbon dioxide and methane, between the atmosphere and the ecosystem over a long multiyear period. In particular, the objective is to understand the duration and magnitude of the exchange mechanisms and environmental drivers for $CO_2$ and $CH_4$ during the whole year (including the shoulder seasons) and their relative importance. Furthermore, this study aims to assess the impact of seasonal thermal anomalies (over the period 1990-2020) on greenhouse gases fluxes. These thermal anomalies serve as critical indicators for evaluating how a shift in temperature pattern influences GHGs emissions and fluxes within the studied ecosystem.

## 2 Methods

### 2.1 Measurement Site

Methane and carbon dioxide turbulent fluxes were measured on the "Amundsen-Nobile Climate Change Tower" (CCT) (Mazzola et al., 2016), located northwest of the village of Ny Ålesund (78°55'N, 11°56'E) in the Spitsbergen Island (Svalbard archipelago - Norway). Measurement campaign started 9$^{th}$ April 2021 until 31$^{st}$ March 2023, for a total of two years. The site is located on the top of a hill, and the land-cover during summer months is characterised by dry tundra or bare soil (Magnani et al., 2022). The climate is typically subarctic with a warming effect by the West Spitsbergen Ocean Current, a branch of the North Atlantic Current. The area is characterised by an average air temperature of about -10 °C in March and 6 °C in July, with about 400 mm of precipitation annually, falling mostly as snow between September and May (Lüers et al., 2014). Wind velocity average is 4.15 m s$^{-1}$, with a maximum monthly average of 5.47 m s$^{-1}$ in December and a minimum in August (2.9 m s$^{-1}$). Wind direction is essentially from three directions, with air masses coming from south-east (42%), south-west (27%) and north/north-west (20%) (see Fig. 1a, inset). A detailed description of the meteorological and micrometeorological conditions for the measurement period was reported, respectively, in Appendix B and Appendix C. CCT area is a semi-desert ecosystem and not wetland or heath tundra (Uchida et al., 2009). The vegetation cover at the measurement site (Fig. A1c) was estimated to be approximately 60%, with the remainder being bare soil with a small proportion of stones (Lloyd et al., 2001).

https://doi.org/10.5194/egusphere-2024-1440
Preprint. Discussion started: 23 May 2024


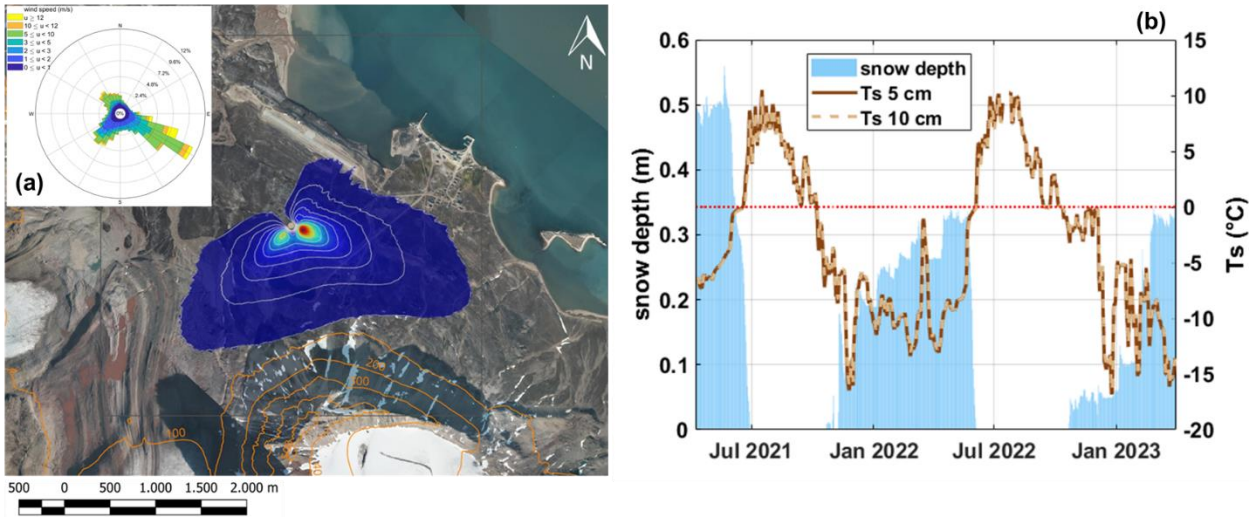


**Figure 1** (a) Location map of the observation site: Ny Ålesund (Svalbard, Norway). Yellow point indicates the Amundsen-Nobile Climate Change Tower (CCT). © Norwegian Polar Institute, www.npolar.no (accessed on 12/03/2024). In the figure it was also reported foreground the flux footprint for the measurement setup (Section 2.3) at 80% contour line. In the inset the wind rose is reported for the period 2010-2023. (b) Soil temperature at two depths (5 cm and 10 cm) on the right axis and snow height (on the left axis) at the CCT site.

The vegetated portion around and within the system footprint area consists of tundra, a widespread ecosystem in Svalbard (Magnani et al., 2022). Specifically, the vegetation is dominated by low-growing vascular plants. This includes various grass and sedge species, such as *Carex* spp., *Deschampsia* spp., *Eriophorum* spp., *Festuca* spp., *Luzula* spp. Additionally, flowering plants like catchfly and saxifrage, as well as woody species like willow, are present. Notably, some locally common species like *Dryas octopetala*, *Oxyria digyna*, and *Polygonum viviparum* are also found (Fig. A1c). A moss and lichen layer are present, though the specific composition remains unclassified (Ohtsuka et al., 2006; Uchida et al., 2009; Lüers et al., 2014). In Ny Ålesund village, the thermal power plant for electricity production is the primary source of $CO_2$. There are few combustion engine cars on the roads and some electric vehicles. The village lacks specific combustion sources, relying entirely on electric facilities. The airport has only two flights per week, and ship arrivals are infrequent, occurring 3-4 times a year, however, cargo handling involves heavy-duty vehicles, and it is moderately active.

### 2.2 Instruments

Standard meteorological data such as air temperature (T) and relative humidity (RH), atmospheric pressure, wind speed and direction were measured at different levels of the CCT (Fig. A1a) by means of the setup described in Mazzola et al. (2016). Snow depth at the foot at the CCT was measured with an ultrasonic range sensor (Campbell Scientific, mod. SR50A), while soil temperature (Ts) was recorded continuously using two temperature probes (Campbell Scientific, mod. 107) positioned at two different depths: 5 cm and 10 cm from the ground level. All sensors were connected to a data logger (Campbell Scientific, mod. CR-3000). Precipitation data for Ny Ålesund were downloaded from the Norwegian Centre for Climate Services web portal (https://seklima.met.no/observations/, last access on 18/03/2024). Radiation components (incoming and

https://doi.org/10.5194/egusphere-2024-1440
Preprint. Discussion started: 23 May 2024


outgoing shortwave and longwave) were measured by means of a radiometer CNR1 (Kipp and Zonen, Netherlands) positioned at 33 m height above the ground with the sensor arm directed towards south.

To measure the eddy covariance (EC) fluxes, a three-dimensional sonic anemometer (WindMaster Pro, Gill) and two open-path gas analysers (LI-7700 for methane and LI-7500A for water vapour and carbon dioxide, both from LI-COR Biogeosciences) were used. All data were recorded at 20 Hz using a SMART Flux interface unit (LI-7550, LI-COR Biogeosciences). The instruments were mounted at a height of 15 m on the CCT above the ground level. Figure A1b shows a typical instrument mounting on the horizontal bar. Air temperature, relative humidity and pressure were also measured by the LI-COR system. The total data coverage during this experiment was 83% for the anemometer, 78% for the Li7500 and 61% for the Li7700, respectively. During this measurement period, a longer break between 8 February and 3 March 2022 was registered in the dataset due to malfunctions in the eddy covariance system. Further, the measurements suffered a break period of 15 days from 5$^{th}$ to 20$^{th}$ February 2023, and stopped for 11 days in December 2022 and March 2023, respectively. Another break period in the dataset must also be included in June 2022 (from the 13$^{th}$ to the 23$^{rd}$) for a total of 10 days. These periods comprise about 10% of the whole dataset.

### 2.3 Eddy Covariance data analysis

Eddy Covariance (EC) vertical turbulent fluxes of GHGs were calculated on a 30 min average using the open-source software EddyPro® package (version 7.0.3; Li-COR Biosciences, USA). The micrometeorological convention of assigning positive values to upward fluxes (emissions) and negative values to downward fluxes (toward the surface) was followed in this work. Spikes in the 20 Hz time series were removed from the dataset and replaced by linear interpolation of neighbouring values using a procedure described by Mauder et al. (2013). Data were discarded when the instrument measurement path became obstructed by water (rain, dew, or snow). Data corresponding to winds blowing from a 260° - 10° sector on the back of the EC setup were excluded from the analysis as they were in the wake of the tower structure (about 18% on the whole dataset). In addition, the diagnostic values of the LI-7700 and LI-7500 gas analysers were used for data quality screening. For the $CH_4$ analyser, LI-7700, the relative signal strength indication (RSSI) was also considered. Methane fluxes were discarded if the mean RSSI of the respective averaging interval was < 20. Spectral corrections were applied to the fluxes using the method described by Fratini et al. (2012). The high and low frequency spectral attenuations were both compensated. The low-frequency loss due to finite averaging time and linear detrending was corrected following Moncrieff et al. (2004). The high-frequency loss due to path averaging, signal attenuation and the finite time response of the instruments was taken into account following (Massmann 2000, 2001). Spectral losses due to crosswind and vertical instrument separation were corrected following Horst and Lenschow (2009). Data at 30 min marked by spikes, drop-outs, discontinuities, or inputs outside absolute limits were discarded from the dataset. Specifically, all data out of the 1st - 99th percentile range was discarded from the subsequent analysis (about 1% of data for each variable). The processing of the raw data included an angle-of-attack correction, i.e. compensation for the flow distortion induced by the anemometer frame (Nakai et al., 2006). To minimise the anemometer tilt error, a three-dimensional coordinate system transformation was

https://doi.org/10.5194/egusphere-2024-1440
Preprint. Discussion started: 23 May 2024


applied to the data set, using the planar fit method proposed by Wilczak et al. (2001). This method ideally results in a null vertical wind component over a long period. The planar fit coefficients are calculated for the month of May (with snow) and August (with bare tundra) in the first and second year. The fit coefficients were calculated over the whole direction sector around the measurement site, spanning 60° wind sector. A linear detrending procedure (Gash and Culf, 1996) was applied to the time series before the calculation of the 30 min average fluxes in order to remove the effects of low-frequency variations and instrument drifts. The Webb-Pearman-Leuning (WPL) correction was applied to compensate for the air density fluctuations, due to thermal expansion or water dilution, to the calculation of the fluxes (Webb et al., 1980; Burba et al., 2008). Further, a correction, considered in the so-called WPL+ module, was applied to consider the broadening of the spectroscopic line for $CH_4$ due to the contemporary presence of the water vapour (McDermitt et al., 2011). An important source of errors is the heat generated by the sensor body of the LI-7500 open-path gas analyser, which may generate convection within the sampling volume (Lafleur and Humphreys, 2007) impacting the calculations of the $CO_2$ fluxes measured by the LI-7500. The correction methods proposed by Burba et al. (2008) yield unrealistic flux values for this data set, especially during winter season, so that we chose not to apply this correction (Lüers et al., 2014). The detection limit (LOD) of the system was obtained using the method proposed by Finkelstein and Sims (2001). For $CO_2$ the LOD value resulted on average 0.3 µmol $m^{-2}$ $s^{-1}$, while for $CH_4$ 1.6 nmol $m^{-2}$ $s^{-1}$. In 16% of the cases, exchange fluxes were lower than the calculated LOD, and by looking at the difference on the cumulated flux values, the contribution of these very low fluxes was of 13 g C $m^{-2}$ (3%) for $CO_2$, and 0.02 g C $m^{-2}$ (5%) for $CH_4$: they were excluded from the final computation, however their inclusion would not have overturned the outcome. The 30-min fluxes underwent quality control based on atmospheric stability and developed turbulence as described by Mauder and Foken (2004). This method was applied to all flux values and classified the dataset into three groups: high quality data (class 0), intermediate quality data (class 1) and low-quality data (class 2 - discarded). Following this procedure, 6% for the momentum flux, about 10% for $CO_2$, $H_2O$, $CH_4$ flux, and 15% for sensible heat flux H were rejected. Some quality indicators derived from the raw data statistics as described by Vickers and Mahrt (1997) were also evaluated. Fluxes related to low turbulence development conditions, i.e. not sufficient to guarantee suitable mixing, need to be identified and filtered out according to the friction velocity value (Aubinet et al., 2012). Such a value was computed (online tool available at https://www.bgc-jena.mpg.de/bgi/index.php/Services/REddyProcWeb - last accessed on 24/11/2023) using the bootstrapping approach described by Reichstein et al. (2005) and Papale et al. (2006), which, in our case, provided u*= 0.042 m $s^{-1}$ and used it to filter the $CO_2$ dataset. Fluxes corresponding to friction velocities lower than the threshold were discarded. Nevertheless, concerning $CH_4$ fluxes, the biological productivity might be a significant environmental factor in determining variability, as suggested in earlier studies (Sachs et al., 2008; Wille et al., 2008). Consequently, no friction velocity threshold was imposed on $CH_4$ data.

The small gaps in the dataset, with duration less than 2 hours were filled by a linear regression (Lüers et al., 2014). Finally, the validated data (as a percentage of the total data point) used in this work adds up to 63% (21,845 points) for H, 48% (16,649 points) for $CO_2$-$H_2O$ flux and 42% (14,555) for $CH_4$ fluxes, respectively. Meteorological variables were gap-filled with ERA5 data. ERA5 is a reanalysis product from the European Centre for Medium-Range Weather Forecast that provides

https://doi.org/10.5194/egusphere-2024-1440
Preprint. Discussion started: 23 May 2024


hourly estimates for various meteorological and soil variables starting from 1959, at a spatial resolution of 25 km (https://www.ecmwf.int/en/forecasts/datasets/reanalysis-datasets/era5, last accessed on 24/03/2023). Each variable was bias-corrected using a linear fit between ERA5 and flux tower observations during periods when both were available. The $CO_2$ and $CH_4$ fluxes time series, as said previously, showed some large gaps (up to 20 days for 2022 winter), thus a gap-filling procedure has also been applied to these time series to avoid biases in the annual flux budgets. Gap filling for $CO_2$ fluxes was implemented, firstly, through the R package REddyProc (https://r-forge.r-project.org/projects/reddyproc/; Reichstein et al., 2005). This gap filling technique, based on Marginal Distribution Sampling (MDS), used as input drivers the incoming shortwave radiation, air temperature, the soil temperature at 10 cm depth, relative humidity, and vapour pressure deficit. However, to take in consideration a complex range of biogeochemical interactions, a random forest regression model of the fluxes was also developed (Kim et al., 2020, Knox et al., 2021) with 12 environmental drivers: sensible and latent heat fluxes, air temperature, soil temperature at 10 cm depth, relative humidity, vapour pressure deficit, air pressure, shortwave incoming and longwave outcoming radiation, the snow depth, the friction velocity and, finally, the boundary layer height. Furthermore, the $CO_2$ flux (gap filled) was itself added as a driver for gap filling the $CH_4$ flux data. Only the gaps in the flux time series are filled with the resulting flux estimates from the random forest regression model. The implementation of the random forest model was developed with an open-source python libraries such as Scikit-learn (Pedregosa et al., 2011). After a process of model tuning the optimal values for various training parameters were found, such as the number of estimators (decision trees) and the maximum depth of the model. Training of the model and model performance estimation were conducted following common methodologies as reported in Dyukarev (2023), which resulted in a validation error (Normalised Root Mean Squared Error) of 7.75% for $CO_2$ and 9.37% for $CH_4$ inference.

The ratio between wind velocity and the friction velocity in neutral atmosphere ($-0.05 < z/L < 0.005$, where z is the measurement height and L is the Obhukov length) was used to evaluate the average roughness length $z_0$, for the site analysed using a parameterisation based on similarity theory (Stull, 1988). The results gave $z_0 = 0.005 \pm 0.001$ m, with similar results reported also by (Mazzola et al., 2021; Donateo et al., 2023 in the same site). Separating the winter period (with snow coverage) from the summer period (without snow), $z_0$ values were calculated as $z_0 = 0.002 \pm 0.001$ m (winter) and $z_0 = 0.004 \pm 0.001$ m (summer), respectively. A null displacement height *d* was considered for this site as obstacles of significant height are not present around the site and in its footprint. Source area for scalar fluxes have been evaluated using a Lagrangian footprint model proposed by Kljun et al. (2015). The results of flux footprint analysis are shown in Fig. 1 with the different influence levels of the zones on the measurements. The gas fluxes measured represented a surface area of about 2.4 $km^2$ (considering the 80% contour line) with a maximum distance of 1300 m and 1600 m in south-west and south-east direction, respectively. It is worth remembering that the data in the wake of the tower structure at north-west and north-east were excluded from the analysis. The flux peak contribution was in the wind direction sectors at about 130 m (± 5 m) at south-east and south-west (Fig. 1). However, the source land area was very similar for the considered wind direction sectors around the measurement site, with 100% of snow coverage for the winter period. During the summer period the footprint area was over tundra coverage, with about 2.4% covered by water surfaces (two arctic lakes) (Fig. 1).

https://doi.org/10.5194/egusphere-2024-1440
Preprint. Discussion started: 23 May 2024


## 2 Results and Discussion

In this work the calendar year was divided into a snow-cover season (winter), a snow-free season (summer), and a thawing/freezing period, in late spring and autumn, respectively. Thawing period represents a transitional phase during which the snow cover melts. Daily soil temperature and snow depth were used to define the different seasons. The start of the snow-cover season was defined as the start of the freeze-up, i.e. the first day on which daily mean Ts at 5 cm depth is below -0.75 °C for 3 consecutive days (Bao et al., 2021; Arndt et al., 2019; Taylor et al., 2018; Zona et al., 2016) and at the same time daily snow depth is greater than 1 cm. The end of the snow-cover season was defined as the start of thaw, i.e. the first date on which daily mean $T_s$ at 5 cm depth rose above 0.75 °C for at least 3 consecutive days. Winter season is between the end of the freezing period and the beginning of the thawing period. At the same time the summer season was defined as the period between the end of thawing (with a snow depth lower than 1 cm) and the beginning of the freezing period. Thawing and freezing periods are also called in the manuscript "shoulder seasons" as reported by Bao et al., 2021. Further, the winter season was divided into a first period (dark winter) in absence of solar radiation (global radiation < 10 W $m^{-2}$) and a second one (light winter) with an increasing global radiation greater than 10 W $m^{-2}$. Thereby two complete light winter (snow-covered) seasons during the study period could be defined: from 1st March 2022 to 19 May 2022 (80 days) and from 5 to 31 March 2023 (27 days). Furthermore, an initial period from 9 April 2021 to 27 May 2021 (48 days) has also been included as a snow-cover period. Two dark winter periods (snow-covered), as specified earlier without solar radiation, have been identified: from 23 October 2021 to 28 February 2022 (128 days) and from 23 October 2022 to 4 March 2023 (132 days). Two complete summer seasons were also included in the dataset: from 29 June 2021 to 07 October 2021 (100 days) and from 4 June 2022 to 13 October 2022 (131 days). Finally, two thawing and freezing periods in 2021 and 2022 were covered in this work. Specifically thawing in the month of May/June and freezing in the month of October for a total of 45 days in thawing and 22 days in freezing period.

### 3.1 $CO_2$ and $CH_4$ mixing ratio

Median $CO_2$ mixing ratio over the whole measurement period was 413.66 ppm (average 412.30 ppm) with an interquartile range (IRQ $25^{th}$ – $75^{th}$ percentile) from 406.17 to 417.72 ppm (Fig. 2a). $CO_2$ mixing ratio is greater during the winter period with a median value of 418.46 ppm decreasing towards the summer season, when it measured a median of 403.81 ppm with a minimum value of 396.61 ppm (Fig. 2b). The shoulder season is characterised by intermediate $CO_2$ concentration: the thawing season showed a median mixing ratio of 415.14 ppm greater than the $CO_2$ concentration in the freezing season (405.62 ppm) (Fig. 2b). The median $CH_4$ mixing ratio for the measurement period was 2.05 ppm (IRQ 2.04 - 2.07 ppm) (Fig. 2c). In this case, the greatest concentration was found during the dark winter season (2.06 ppm) with a decreasing trend going towards the summer season down to a median value of 2.05 ppm. The thawing and freezing seasons presented very similar values in $CH_4$ concentration; 2.044 and 2.043 ppm, respectively (Fig. 2d).

https://doi.org/10.5194/egusphere-2024-1440
Preprint. Discussion started: 23 May 2024


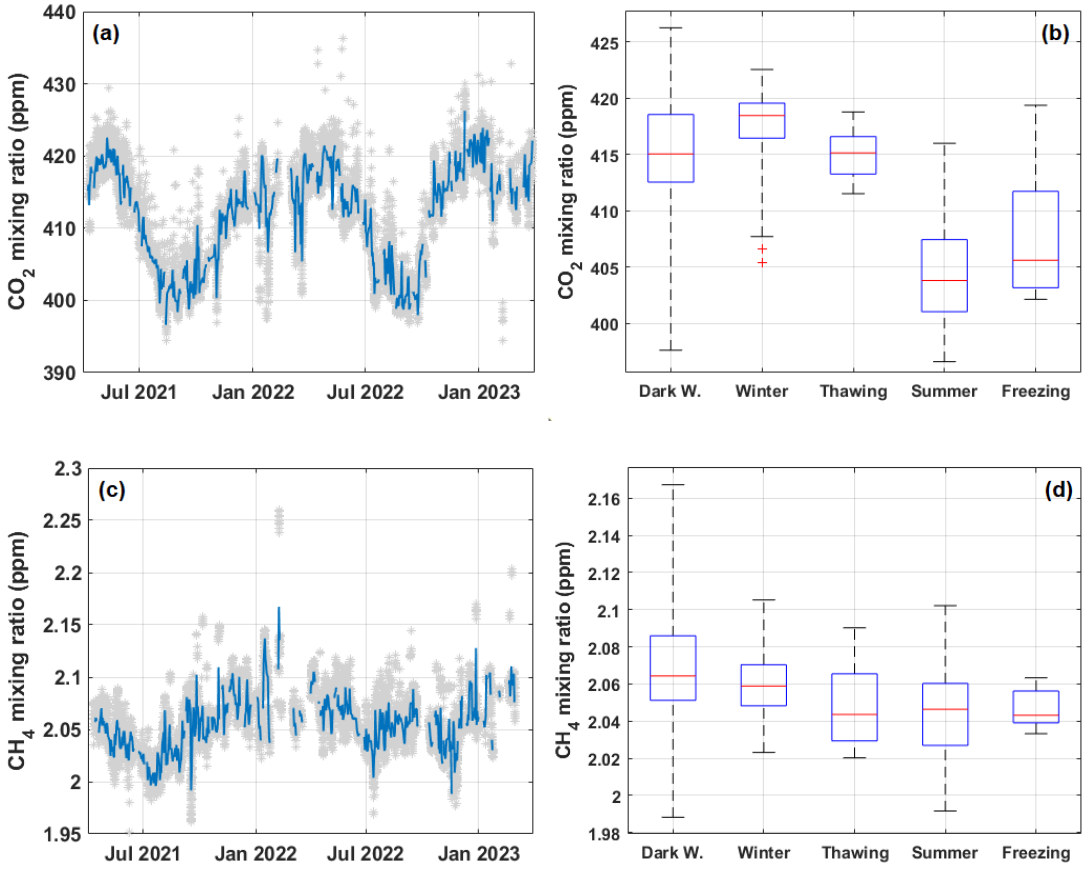


**Figure 2** Time series on a daily basis (left) and whiskers-box plots (right) of (a,b) $CO_2$ and (c,d) $CH_4$ mixing ratio. In the left panels, in light grey the time series for $CO_2$ and $CH_4$ mixing ratio at 30 min resolution. In the right panels, whiskers represent max and min values, the box limits are the 25th and 75th percentiles. The red line represents the median value on a 30 min basis.

In Fig. 3a,c, the annual cycle of $CO_2$ and $CH_4$ turbulent fluxes is observed, with $CO_2$ and $CH_4$ fluxes exhibiting negative intensity for the great part of the year. $CO_2$ flux has a median value for the whole period of -0.11 µmol $m^{-2}$ $s^{-1}$ (detailed statistics in Table 1). At the same time, the median value for the $CH_4$ flux was -0.39 nmol $m^{-2}$ $s^{-1}$ (Table 1). Negative values are particularly important in $CO_2$ and $CH_4$ fluxes during the summer season (growing season) indicating a sink behaviour for the CCT site.

**Table 1** Statistical analysis for the $CO_2$ and $CH_4$ fluxes in the measurement site separated into five different seasons defined in this work.

| | **$CO_2$ flux (µmol $m^{-2}$ $s^{-1}$)** | | | | |
|---|---|---|---|---|---|
| | **Dark W.** | **Light W.** | **Thawing** | **Summer** | **Freezing** |
| mean | -0.076 | -0.275 | -0.360 | -0.453 | -0.136 |

https://doi.org/10.5194/egusphere-2024-1440
Preprint. Discussion started: 23 May 2024


| | | | | | |
|---|---|---|---|---|---|
| median | -0.103 | -0.252 | -0.176 | -0.372 | -0.171 |
| 25$^{th}$ percentile | -0.236 | -0.424 | -0.538 | -0.774 | -0.246 |
| 75$^{th}$ percentile | 0.084 | -0.055 | -0.081 | -0.130 | -0.052 |
| min | -0.914 | -3.044 | -1.589 | -1.951 | -0.386 |
| max | 0.772 | 0.416 | 0.188 | 0.515 | 0.38 |

| **$CH_4$ flux (nmol $m^{-2}$ $s^{-1}$)** | | | | | |
|---|---|---|---|---|---|
| mean | -0.368 | -0.665 | -0.972 | -1.375 | -0.498 |
| median | -0.175 | -0.359 | -0.83 | -1.284 | -0.688 |
| 25$^{th}$ percentile | -0.958 | -1.018 | -1.512 | -2.292 | -1.424 |
| 75$^{th}$ percentile | 0.302 | 0.043 | -0.055 | -0.467 | 0.137 |
| min | -4.599 | -7.271 | -5.594 | -5.319 | -3.202 |
| max | 6.993 | 1.779 | 1.207 | 2.673 | 1.842 |

Seasonal analysis reveals negative median values for the fluxes of both $CO_2$ and $CH_4$, peaking in summer with -0.37 µmol $m^{-2}$ $s^{-1}$ and -1.28 nmol $m^{-2}$ $s^{-1}$, respectively. Jørgensen et al. (2015) field measurements, within the Zackenberg Valley in northeast Greenland over a full growing season, show methane uptake with a seasonal average of -2.3 nmol $CH_4$ $m^{-2}$ $s^{-1}$ in dry tundra. Wang et al. (2013) observed a net uptake of $CH_4$ with an average uptake flux of −2.7 nmol $m^{-2}$ $s^{-1}$ at a temperate forest (Haliburton Forest and Wildlife Reserve) in central Ontario from June to October 2011. $CO_2$ fluxes showed slightly negative median values also in winter (-0.10 and -0.25 µmol $m^{-2}$ $s^{-1}$) and shoulder seasons (-0.18 for the thawing and -0.17 for the freezing period). However, the $CO_2$ flux trend indicates the presence of positive fluxes (emissions) at 30 min resolution, especially during the dark/light winter and the freezing period (Table 1). A similar trend is reported for methane: during dark/light winter methane fluxes are negative with a median value of -0.17 and -0.36 nmol $m^{-2}$ $s^{-1}$, respectively. However, looking at the winter season (Table 1), the presence of some significant emission phenomena can be argued for the site. In contrast, these phenomena diminished in the shoulder seasons, where significant absorption events prevailed with -0.83 nmol $m^{-2}$ $s^{-1}$ during thawing and -1.3 nmol $m^{-2}$ $s^{-1}$ during freezing period. In the same season, Wang et al. (2013) measured a drop in the $CH_4$ uptake to an average of −2.95 nmol $m^{-2}$ $s^{-1}$.

https://doi.org/10.5194/egusphere-2024-1440
Preprint. Discussion started: 23 May 2024


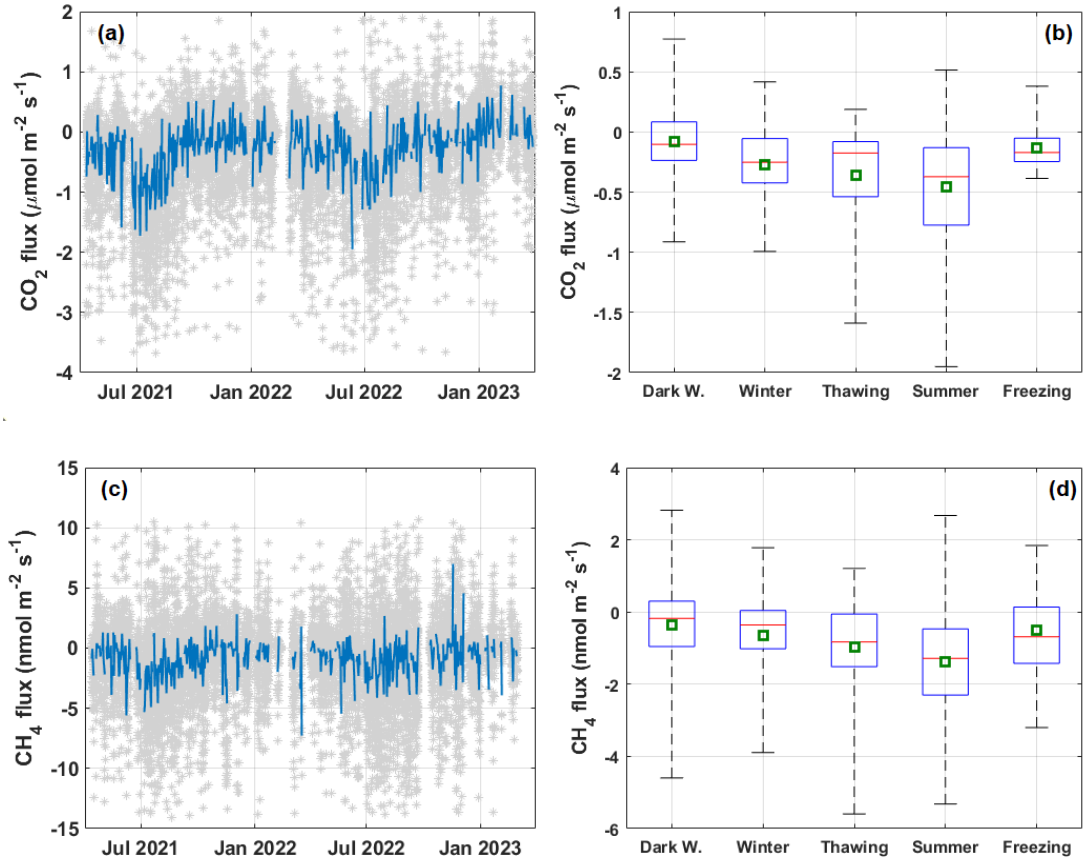


**Figure 3** Time series on a daily basis (left) and whiskers-box plots (right) of turbulent vertical flux (a,b) $CO_2$ and (c,d) $CH_4$ measured at CCT. In the left panels, in light grey the time series for $CO_2$ and $CH_4$ mole fraction at 30 min resolution. In the right panels, whiskers represent max and min values, the box limits are the 25$^{th}$ and 75$^{th}$ percentiles. The red line represents the median value and the green square the average value.

Even a similarity between the $CO_2$ and $CH_4$ flux patterns can be observed from the time series, the exchange processes are probably led by different physical drivers. The significantly negative fluxes of $CO_2$ are driven by the process of photosynthesis, while the absorbing negative fluxes of $CH_4$ are generally related to an increase of the soil temperature. Overall, it was observed that absorbing $CH_4$ fluxes increases significantly in coincidence with a peak in ground temperatures, which occur predominantly during the summer season.

### 3.2 $CO_2$ and $CH_4$ mass budget

The cumulative mass budget over the two years for the CCT site ecosystem are shown in Fig. 4. Based on the budget for the whole measurement period, the study area acts as a net sink for both $CO_2$ and $CH_4$. A sink $CO_2$ budget of close to -345 gC m$^{-2}$ was found over the study period, whereas the $CH_4$ uptake contribution was estimated to be around -0.36 gC m$^{-2}$. Actually,

https://doi.org/10.5194/egusphere-2024-1440
Preprint. Discussion started: 23 May 2024


for the best evaluation of the cumulated carbon quantity, it should be better to consider the gap filled time series (both with MDS and RF methodology) as seen in Section 2.3. In this perspective, the total cumulative $CO_2$ budget over the measurement campaign was -673 gC $m^{-2}$ with MDS and -735 gC $m^{-2}$ using the RF procedure, respectively (Fig. 4a). On the other hand, $CH_4$ cumulative budget was of about -0.77 gC $m^{-2}$ with the RF gap filling procedure (Fig. 4b). The mean annual cumulative $CO_2$ budget was -173 gC $m^{-2}$ with MDS data filling procedure and -189 gC $m^{-2}$ with RF. On average, the annual cumulative budget for $CH_4$ was -0.17 gC $m^{-2}$ with RF data (Table 2). Treat et al. (2016) found a median annual value of 0.20 gC $m^{-2}$ on tundra uplands. The annual budget can be further detailed into the five seasons considered in this study. Specifically, the CCT area acted as a $CO_2$ sink during the thawing and summer period with an average value of -0.82 and -1.1 gC $m^{-2}$ $day^{-1}$, respectively. During the freezing period the quantity of absorbed $CO_2$ per day decreased down to -0.34 gC $m^{-2}$ $day^{-1}$, coming to almost null value during the winter period (-0.16 gC $m^{-2}$ $day^{-1}$ for dark winter and -0.52 gC $m^{-2}$ $day^{-1}$ for light winter). The same pattern was followed by the $CH_4$ absorbed carbon mass: in this case during the thawing period was observed a value on average of -0.54 mgC $m^{-2}$ $day^{-1}$, peaking its maximum during the summer period (-1.22 mgC $m^{-2}$ $day^{-1}$). Also, in this case the absorbed carbon mass decreases in the freezing period down to -0.66 mgC $m^{-2}$ $day^{-1}$. It was reduced to very low values during the winter season with -0.30 mgC $m^{-2}$ $day^{-1}$ in dark winter and -0.40 mgC $m^{-2}$ $day^{-1}$ in light winter.

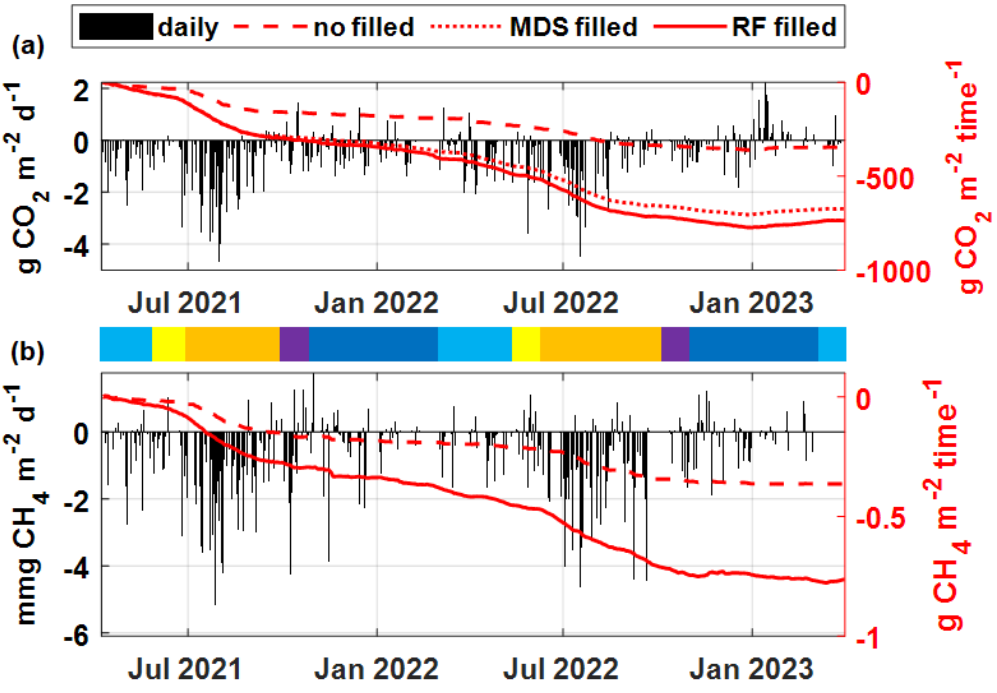


**Figure 4** Daily (black bars - left axis) and cumulative (red - right axis) ecosystem exchange for (a) $CO_2$ and (b) $CH_4$ measured at CCT site. Central multicoloured bar separates the time series into five different seasons: blue for light winter, yellow for thawing, orange for summer, purple for freezing and navy for dark winter.

https://doi.org/10.5194/egusphere-2024-1440
Preprint. Discussion started: 23 May 2024


345

**Table 2** Mean cumulated $gCO_2$ and $gCH_4$ for each season defined in this work and the mean cumulated $gCO_2$ and $gCH_4$ yearly in the measurement site. The values are reported for the original gap time series (RAW), the gap-filled dataset with MDS and RF procedure.

| | $CO_2$ cumulated ($gCO_2$ $m^{-2}$) | | | | | |
|---|---|---|---|---|---|---|
| | **Dark W.** | **Light W.** | **Thawing** | **Summer** | **Freezing** | **Year** |
| **RAW** | -13.06 | -14.59 | -4.98 | -66.02 | -2.67 | -84.73 |
| **MDS** | -25.68 | -27.16 | -33.48 | -126.51 | -3.44 | -172.63 |
| **RF** | -32.52 | -28.05 | -35.33 | -132.10 | -4.07 | -189.35 |
| | $CH_4$ cumulated ($mgCH_4$ $m^{-2}$) | | | | | |
| **RAW** | -13.78 | -7.47 | -3.99 | -73.69 | -7.15 | -77 |
| **RF** | -28.06 | -26.91 | -32.34 | -132.42 | -9.50 | -178 |

350

### 3.3 Physical drivers on GHGs surface fluxes

Previous works have shown that advection, forced by wind pumping related to atmospheric turbulence and site energy balance, can increase turbulent fluxes from/to the snowpack (Sievers et al., 2015). Typically, this wind pumping effect led to increased emissions flux in $CO_2$ and $CH_4$ resulting from ebullition and/or ventilation. This correlation is analysed for the
355 snow-covered periods (dark/light winter) in our measurement site. The scatter plot in Fig. 5a shows a positive correlation between wind speed and vertical turbulent $CO_2$ flux, with a clear increasing relationship indicating positive fluxes for wind speed above 8 m $s^{-1}$. Further, an anti-correlation can be observed in Fig. 9b, where the sensible heat flux H is plotted against the $CO_2$ turbulent flux. This counter correlated behaviour is strictly a consequence of the connection between ice surface cooling (or warming) and $CO_2$ outgassing (or uptake). A similar dependence was also observed on sea ice in a coastal fjord
360 environment in northeast Greenland (Sievers et al., 2015) and on Antarctic sea ice (Zemmelink et al., 2006).

https://doi.org/10.5194/egusphere-2024-1440
Preprint. Discussion started: 23 May 2024


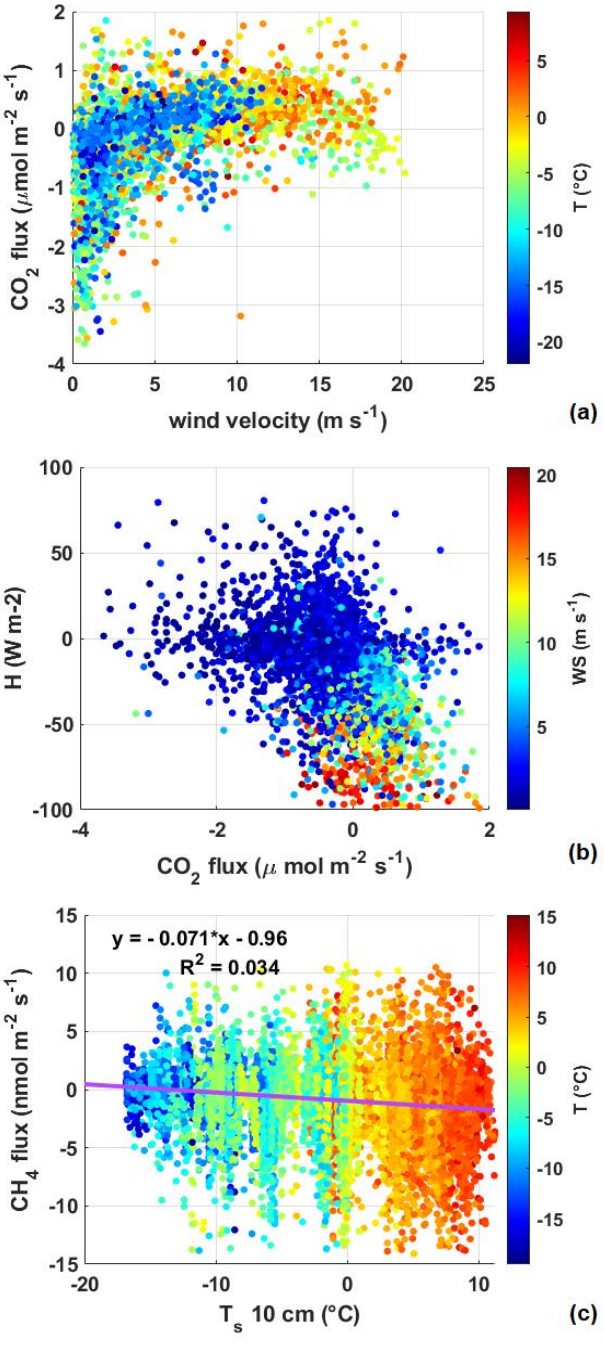


**Figure 5** (a) Scatter plot of turbulent vertical $CO_2$ flux against wind speed. Data is colour-coded according to air temperature T. (b) Scatter plot of the sensible heat flux H against turbulent vertical $CO_2$ flux. In this case, data is colour-coded according to wind speed (WS). (c) Scatter plot of the vertical $CH_4$ flux as a function of Ts. Data is colour-coded according to air temperature T. In panel (a) and (b) data was selected for snow cover period (dark/light winter).

https://doi.org/10.5194/egusphere-2024-1440
Preprint. Discussion started: 23 May 2024


At CCT, where uptake seems to outweigh emission within the flux footprint, a reversal in methane concentration gradient can be observed. This means that the soil layer would be relatively depleted in methane compared to the atmospheric boundary layer. The coarse soils at CCT may therefore experience increased aeration, which could in turn aid in the transportation of $CH_4$-rich air from the overlying atmosphere to the methanotrophs, and/or enhance the movement of $CH_4$-depleted air from the soil into the atmosphere. In addition, increased aeration would provide oxygen to the deeper soil layers during the dry season, stimulating the activity of aerobic methanotrophs. In addition to known groups of aerobic methanotrophs described in Svalbard and other Arctic regions (Wartiainen et al., 2006a,b; Christiansen et al., 2015; Yun et al., 2023), low affinity methanotrophs capable of oxidising methane at low concentrations have been described and identified in diverse ecosystems, including the Arctic (Greening and Grinter, 2022; Yun et al., 2023). Given the mineral-rich soils nature of the investigated area and of a large portion of the Arctic ecosystem, methane oxidation by aerobic methanotrophs in these dry and mineral soils plays an important role in reducing the methane net emission to the atmosphere in the Arctic.

Prior research has demonstrated the influence of soil temperature on methanotrophic activity (Reay et al., 2007); nevertheless, $CH_4$ fluxes at CCT exhibited a limited association with soil temperature. Analysis through a scatter plot (Fig. 5c) depicting $CH_4$ flux alongside both soil and ambient temperatures revealed minimal correlation in contrast to other environmental factors, indicating that variations in temperature had minimal impact on $CH_4$ fluxes. The extent to which temperature fluctuations affect $CH_4$ fluxes in the soil is heavily contingent on the depth of the microbial community responsible for these fluxes. Despite previous findings indicating that methanotroph habitats are typically situated near the soil surface at depths ranging from 3 to 15 cm (Curry, 2007; Yun et al., 2023), there was no assessment of the vertical distribution of microbial populations in the soil at the CCT site. The lack of correlation with soil temperature might be further due to the psychrophilic nature of the methanotrophic communities in the Arctic soils. Overall, the observed correlation in the ecosystem uptake of methane with wind velocity suggests that the methanotrophic communities in the Svalbard soils might be electron acceptor limited and are stimulated by soil aeration.

### 3.4 GHGs fluxes response to seasonal temperature anomalies

In this work the seasonal temperature anomalies were evaluated as possible drivers for the modifications in GHG exchange turbulent fluxes on a daily basis. This approach allowed for a comprehensive understanding of the relationship between thermal variations and corresponding flux dynamics over the considered time period. In this study, temperature anomalies were calculated with respect to the average values over the period 1991-2020 as baseline. Figure 6 depicts the dependence of the $CO_2$ and $CH_4$ turbulent fluxes on the temperature anomalies, on a daily basis, based on a 5-day running window. As can be observed, net uptake fluxes for both gases are most noticeable in conditions of near-zero and above-zero ground temperatures (clearly indicating the summer period) but with thermal anomalies below 5°C. The magnitude of negative fluxes decreases with increasing positive thermal anomalies during both wintertime and summer until it reverses to a positive (emissive) flux for anomalies above 10°C, especially during wintertime. At the same time, GHG fluxes remain moderately or just slightly negative for pronounced negative anomalies (< -5°C) (Fig. 6a). A similar pattern was observed during summer,

https://doi.org/10.5194/egusphere-2024-1440
Preprint. Discussion started: 23 May 2024


albeit within a lower anomaly range. This behaviour suggests that the trend is toward a zero uptake of $CO_2$, considering the increasing frequency and intensity of positive temperature anomalies, especially in the winter period. At the same time, $CO_2$ absorption during summer seems to be attenuated in the case of marked positive anomalies. Figures 6c,d, shows the same type of analysis for $CH_4$ fluxes, which shows a consistent uptake for both positive temperature anomalies (below 10°C) and for temperature around 0°C, and very low fluxes for negative anomalies (below -5 °C). In contrast, a similar pattern to that observed for $CO_2$ occurred during summertime, with sharp uptake fluxes for thermal anomalies below 5 °C. Shoulder seasons show a positive trend between fluxes and thermal anomalies, albeit based on a tight range of thermal anomalies. Specifically, during the freezing season, absorption and emission fluxes occur with negative and positive anomalies, respectively, whereas negative fluxes were observed during thawing periods. In a context of climate change, large positive anomalies could lead to emission conditions in all seasons, while optimal situations could occur during the summer, considering a lower temperature increase in this season (Bintanja and Linden, 2013). Overall, $CO_2$ exhibits emissions fluxes, particularly during winter, with attenuated absorption fluxes in summertime. The results suggest a transition of $CO_2$ flux regimes for thermal anomalies above 10°C during different seasons. The findings in this study align with the observed decrease in the net carbon reservoir in northern ecosystems as air temperature rises (Cahoon et al., 2012; Zona et al., 2022).

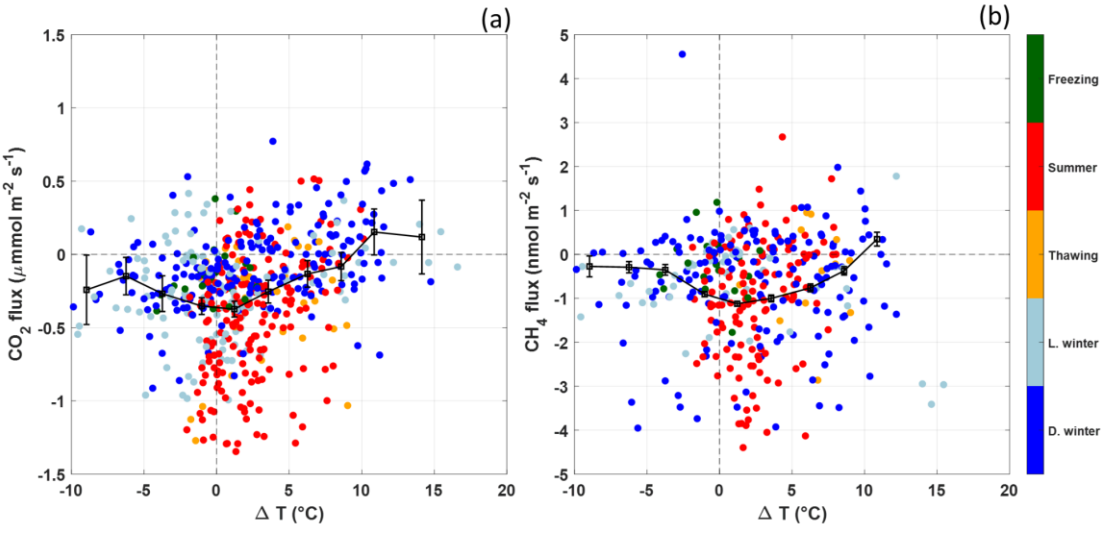


**Figure 6** (a) $CO_2$ vertical fluxes vs temperature anomalies. (b) $CH_4$ vertical fluxes against temperature anomalies for the different seasons. Data is colour-coded according to different seasons identified in this work.

## 4. Conclusions

In this study, $CO_2$ and $CH_4$ turbulent fluxes on tundra ecosystems in the Svalbard Island (Norway) were investigated, using a two-year measurement campaign. The observed absorption/emission patterns in both $CO_2$ and $CH_4$ underscore the dynamic interplay between climatic conditions and ecosystem activities (such as photosynthesis and microbial activity) at the measurement site. During the summer season, the pronounced uptake flux (for both carbon dioxide and methane) suggests an

https://doi.org/10.5194/egusphere-2024-1440
Preprint. Discussion started: 23 May 2024


increase in mosses and lichens photosynthesis and/or microbial methane consumption, while the transition to neutral or null fluxes in the freezing season and in winter indicates a decrease in these activities. The enhanced methane uptake during the melting period aligns with the activation of soil microorganisms and correlates with increasing aeration of the topsoil. $CO_2$ absorption intensified in the summer season, while during October the decreasing photosynthetic activity, together with the first occurrence of the snow, led to a sensible reduction of absorbing phenomena giving way to the ecosystem respiration and relatively low negative $CO_2$ fluxes. During the winter period the processes forcing $CO_2$ accumulation and $CO_2$ release counterbalance each other, resulting in very low negative flux, reducing any further biological activity. The methane budget shows a sink behaviour for the measurement site, especially for the summer season gradually approaching neutral during the freezing season. The methane uptake decreases during the winter season due to the presence of the snow and the methanotrophic activity is nearly stopped by negative soil temperature. Methane uptake rate rises again during the melting period started by the activation of soil methanotrophic microorganisms. $CH_4$ fluxes at CCT exhibited a limited association with both soil and ambient temperatures in contrast to other environmental factors. The lack of correlation with soil temperature might be further due to the psychrophilic nature of the methanotrophic communities in the Arctic soils. Overall, the observed correlation in the ecosystem uptake of methane with wind velocity suggests that the methanotrophic communities in the Svalbard soils might be electron acceptor limited and are stimulated by soil aeration. The analysis of the impact of thermal anomalies on $CO_2$ and $CH_4$ exchange fluxes, underscores that high thermal anomalies may contribute to an increased positive flux for $CO_2$. The intensity of increasing temperature anomalies may limit the peak summer productivity of plants, decreasing the ability of these ecosystems to sequester carbon. These results can serve as a reference for models examining the dynamics of tundra ecosystems in response to climate change. In the case of methane, absorption fluxes are generally observed for positive anomalies, especially during wintertime. The implications of these results contribute valuable insights to our understanding of ecosystem responses in the face of evolving climatic conditions. Further research is needed to better understand the sources and sinks of these GHGs in the dry tundra ecosystem, to develop effective mitigation strategies to reduce their impact on the local and global climate.

## Appendix A: Climate Change Tower (CCT)

https://doi.org/10.5194/egusphere-2024-1440
Preprint. Discussion started: 23 May 2024


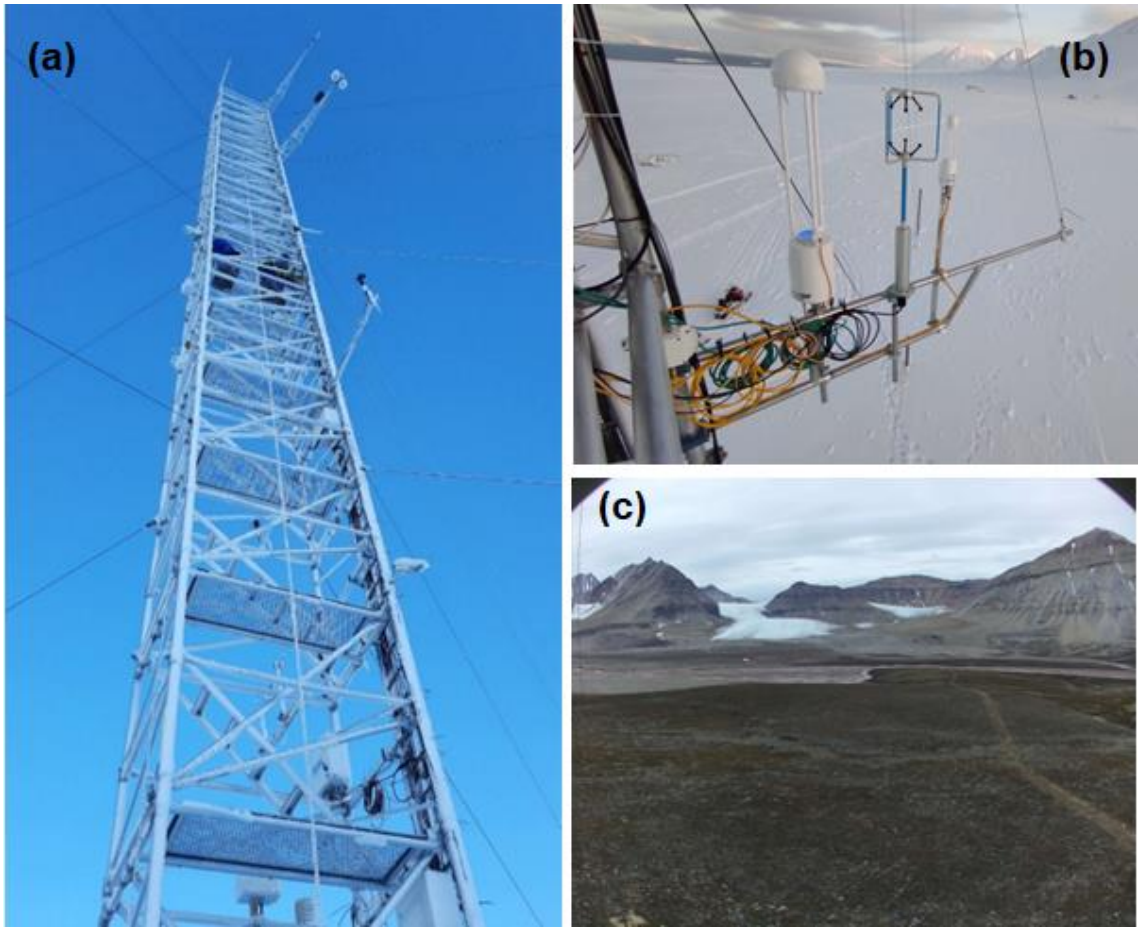


**Figure A1** (a) Climate Change Tower (CCT) picture with several instrumentations installed at different heights. (b) A picture of the EC installation setup with Li7700 (left), sonic anemometer (middle) and Li7500A (right) on the steel horizontal bar. c) A bird's-eye view of the tundra in the CCT site. Photo courtesy of Roberto Salzano (CNR-IIA).

## Appendix B: Meteorology at CCT for the measurement period

The mean air temperature was of −1.3 °C (+/- 7 std. dev) during the measurement period. March records the lowest T, with a daily average of -20.3 °C (see Fig. B1a), while from April onwards, T gradually rises, peaking at 13.5 °C daily in July. At the same time, RH reached its maximum value of 93%, maintaining high levels throughout August (Fig. B1c). The minimum RH value of 31% (on a daily basis) was recorded in April. Solar radiation (both global and net radiation) takes on positive values greater than 10 W $m^{-2}$ from the month of February (starting halfway through) until the month of October (to about the 15th) (Fig. B1e). The total precipitation in the area for the two-year period was distributed as 235 mm in 2021 (from April to December), 573 mm in 2022 and 160 mm in 2023 (January-March only). Global solar radiation (shortwave incoming radiation), which is one of the main drivers for the photosynthesis processes, shows relatively high median values for thawing and winter season (226 W $m^{-2}$ and 120 W $m^{-2}$, respectively), and decreasing values for summer (88 W $m^{-2}$) and

https://doi.org/10.5194/egusphere-2024-1440
Preprint. Discussion started: 23 May 2024


freezing (4.5 W $m^{-2}$) (Fig. B1e). Note that during dark winter the global radiation is very low, actually null, as this period has been defined. Snowpack in the first period until 27th of May 2021 has an average depth of 0.41 m with a maximum peak at 0.56 m in 2021. In 2022 and 2023 the depth of the snowpack is lower, with an average depth of 0.24 m and 0.14 m, respectively (Fig. 1b). The maximum snowpack depth in the last two years is 0.35 m. The snow is largely spread by wind, as is typical for such areas on Svalbard (Winther et al., 2003). Overall, the ground is covered by snow for 62% of the measurement period. The average difference between Ts at 5 cm and Ts at 10 cm is 0.006 °C, with an absolute average gradient over the whole period of 0.12 °C $m^{-1}$ (Fig. 1b). The maximum Ts is 15 °C (in July), the minimum -16 °C (in December 2022). In this work a particular focus was placed on both the study of shoulder seasons as well as on winter and summer seasons. The temperature differences between the selected seasons are significant. Specifically, the winter period T (Fig. B1b) is sharply below zero (median -6.51 °C). The lowest cumulative precipitation (only rain) was observed in the freezing period (20 mm), while during the dark winter the total rainfall accounted for 522 mm, up to 53 mm on a daily basis, with four rain days for a total of 136 mm, corresponding to 26% of the dark winter total. Thawing period T was in milder conditions, with a median value of 2.92 °C (0.41-8.81 °C, min-max), while the warmest temperatures were observed during the summer season, even exceeding 5°C on median values (with a maximum of 13.47 °C) (Fig. B1b). Simple Daily Intensity Index (SDII) was calculated to provide information about the intensity of precipitation on days with rainfall. SDII computes the average amount of rainfall (mm) per day, offering a perspective on the strength of precipitation and indicating its intensity. Analysing the SDII index (Lucas et al., 2021), the thawing period recorded the highest value (7.4 mm day-1) with an absolute rainfall of 37 mm, followed by the dark winter period (6.6 mm day-1), while the lowest value (2.9 mm d-1) was observed during the freezing period, suggesting lighter rainfall on rainy days (Fig. B1h). High RH conditions (up to a median of 72 %) are prevailing during the summer season (Fig. B1d) with a cumulative precipitation of 230 mm (SDII 5.6 mm d-1). The freezing period is generally characterised by temperatures that can reach a median of -4.35 °C in October, with RH reaching a minimum of 46 %.

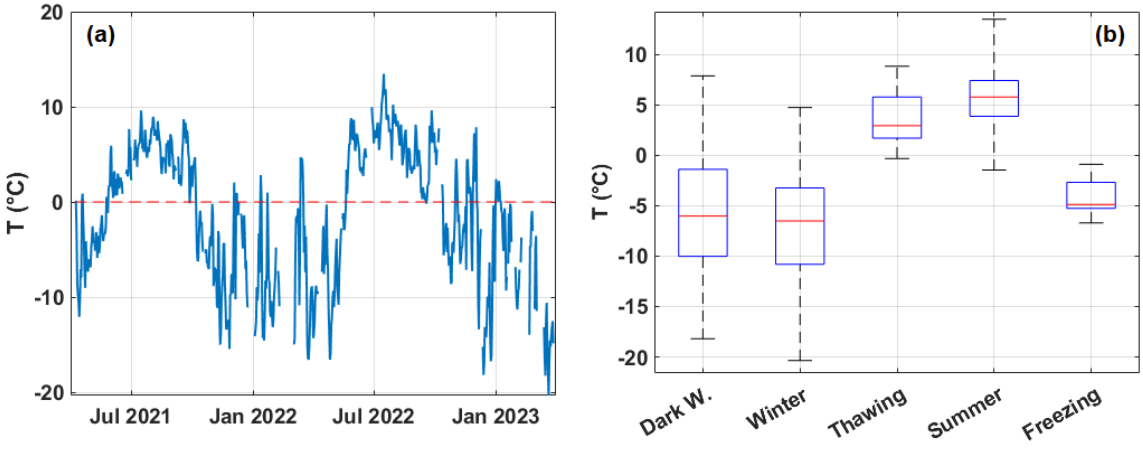

https://doi.org/10.5194/egusphere-2024-1440
Preprint. Discussion started: 23 May 2024


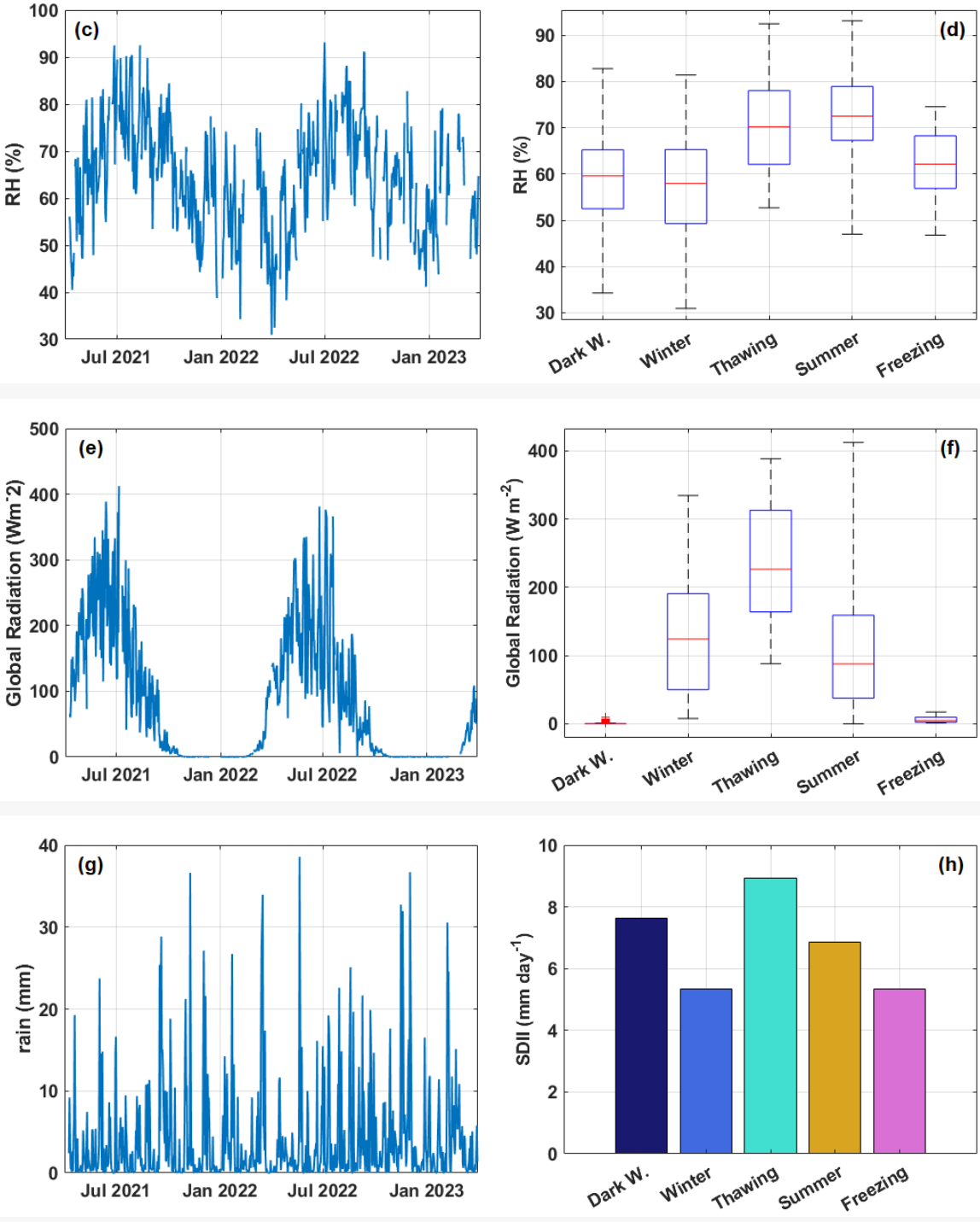


485

**Figure B1** Time series and box plot with whiskers on daily and seasonal basis respectively of (a-b) temperature (°C); (c-d) relative humidity (%); (e) downwelling and upwelling shortwave and longwave radiation (W $m^{-2}$) and (f) SDII (mm $d^{-1}$) at

https://doi.org/10.5194/egusphere-2024-1440
Preprint. Discussion started: 23 May 2024


CCT site. In the right panels, whiskers represent max and min values, the box limits are the 25$^{th}$ and 75$^{th}$ percentiles. The red line represents the median value on a 30 min basis.

**Appendix C: Micrometeorology at CCT for the measurement period**

In the measurement period, sensible heat flux was on average negative (- 6 W m$^{-2}$), on a daily basis (Fig. C1a). The results show the presence of a long period with negative energy fluxes from freezing to thawing season and a minimum around -77 W m$^{-2}$ until snow cover is present and during the melting snow phase, when the atmosphere is warmer than the surface. Sensible heat flux values had a positive magnitude (directed toward the atmosphere) for 32.7% of cases and for 67.3% of events it was directed toward the snowpack. Upon thawing, a positive sensible heat flux becomes evident (see Fig. C1b), exhibiting median values of 4.2 W m$^{-2}$ (max 47 W m$^{-2}$) in July, corresponding to the peak net solar radiation (253 W m$^{-2}$) observed throughout the year. This behaviour has previously been observed in the Arctic (Kral et al., 2014; Donateo et al., 2023) where the snowpack acts as a sink of heat during the winter and spring months. In the freezing period, sensible heat fluxes are negative (median -6.04 W m$^{-2}$), down to -26 W m$^{-2}$ on daily averages, indicating energy moving toward the surface (Fig. C1b). Latent heat flux (Fig. C1c,d) has its minimum median value during the winter (light winter with a median of 1.19 W m$^{-2}$), while its maximum median on season basis was reached during the summer (14.32 W m$^{-2}$). Intermediate values were registered during the shoulder seasons, with 1.19 W m$^{-2}$ and 2.4 W m$^{-2}$ during thawing and freezing, respectively. In general, in this dataset no significant correlation between methane and latent heat fluxes has been observed (not shown here). Latent heat flux was positive for 76.2% of the cases, while it was directed toward the soil in 23.7% of cases. The median measured latent heat flux was 2.93 W m$^{-2}$ (8.48 W m$^{-2}$ on average) during the observation campaign. In Fig. C1e the time series of friction velocity shows a mean value of 0.19 m s$^{-1}$ on the whole measurement period. No specific differences can be noted in the friction velocity behaviour due to the changing in snowpack characteristics or through the selected seasons. During winter, the friction velocity oscillated around a median value of 0.16 m s$^{-1}$. Thawing median value was slightly lower (about 0.13 m s$^{-1}$), while during summer the maximum values reached 0.15 m s$^{-1}$ (Fig. C1f). In particular, the frequency of stable and highly stable atmospheric conditions is 54% and 13%, respectively, of the total cases; while unstable and highly unstable conditions occur for 20% and 12%, respectively. Finally, neutral conditions are rare, showing a frequency below 1%. Atmospheric stable conditions prevail for the whole year, especially during the Arctic night (with a maximum stability parameter of 1.8). During dark and winter seasons, stable and very stable conditions are predominant (65% and 16%, respectively). Unstable atmospheric conditions arise only during the summer period with a median stability parameter of 0.47. In summer, there is a prevalence of unstable (33%) and very unstable (20%) conditions, with very stable cases below 10%. The thawing season also exhibits a predominant stable situation (with 69% of stable and very stable cases) with a median stability parameter of 0.22. The freezing season shows a stability frequency distribution like the previous shoulder season, with a higher prevalence of stable cases (60%).

https://doi.org/10.5194/egusphere-2024-1440
Preprint. Discussion started: 23 May 2024


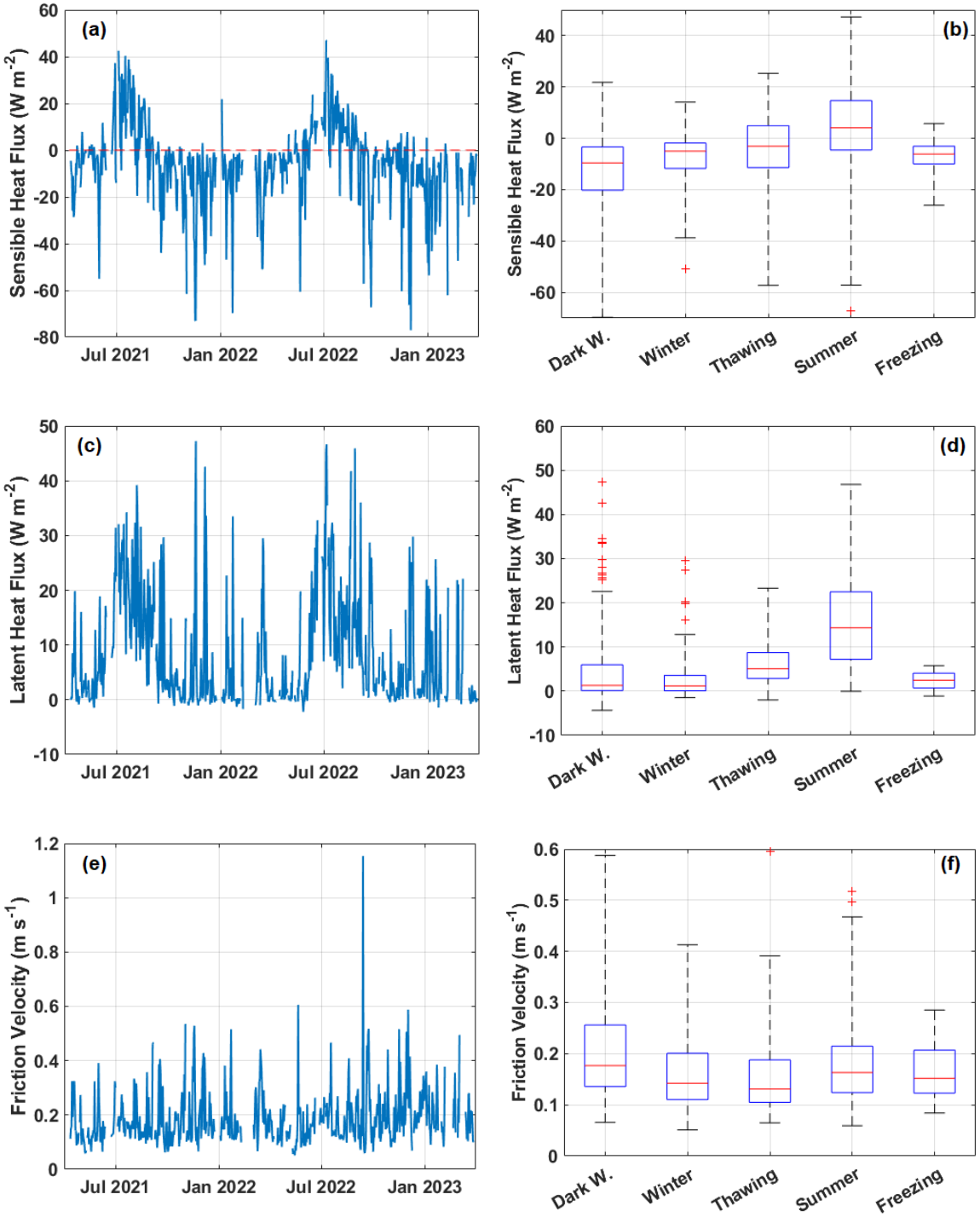


**Figure C1** Time series on a daily basis (left) and whiskers-box plots (right) of the principal micrometeorological variables measured during the campaign. (a,b) Sensible heat flux (W $m^{-2}$); (c,d) latent heat flux (W $m^{-2}$) and (e,f) friction velocity (m $s^{-}$

https://doi.org/10.5194/egusphere-2024-1440
Preprint. Discussion started: 23 May 2024


[1]). In the right panels, whiskers represent max and min values, the box limits are the 25th and 75th percentiles. The red line represents the median value on a 30 min basis.

*Data availability*: The data that support the findings of this study are openly available in the Italian Arctic Data Center (IADC) at https://doi.org/10.48230/DSET.2024.0001 (Donateo et al., 2024).

*Author contributions*: **AD**: Conceptualization; instrumental setup, data collection and post-processing, data curation; formal analysis; investigation; methodology; visualisation; writing – original draft, funding acquisition; project administration; supervision. **DF**: data curation; formal analysis; investigation; methodology; writing – review and editing. **DG**: Investigation; methodology; writing – review and editing. **AM**: Data curation; formal analysis; investigation; methodology; writing – review and editing. **MM**: Instrumental setup, data collection and post-processing, data curation; writing – review and editing. **SD**: investigation; methodology; writing – review and editing, funding acquisition; project administration; **GP**: Conceptualization; instrumental setup, data collection and post-processing, data curation; formal analysis; investigation; methodology; visualisation; writing – original draft.

*Competing interests*: The authors declare that they have no conflict of interest.

*Acknowledgements:* This work has been conducted in the framework of the Joint Research Agreement ENI-CNR, WP1 "Impatto delle emissioni in atmosfera sulla criosfera e sul cambiamento climatico nell'Artico". The Authors wish to thank the staff of CNR-ISP for the logistical support at Arctic Station "Dirigibile Italia" in Ny Ålesund.

## References

AMAP, 2021. AMAP Assessment 2021: Impacts of Short-lived Climate Forcers on Arctic Climate, Air Quality, and Human Health. Arctic Monitoring and Assessment Programme (AMAP), Tromsø, Norway. x + 375pp. ISBN – 978-82-7971-202-2.

Arndt, K. A., Oechel, W. C., Goodrich, J. P., Bailey, B. A., Kalhori, A., Hashemi, J., Sweeney, C., and Zona, D.: Sensitivity of methane emissions to later soil freezing in Arctic tundra ecosystems, J. Geoph. Res.: Biogeosciences, 124 (8), 2595–2609, https://doi.org/10.1029/2019J G005242, 2019.

Arnold, S. R., Law, K. S., Brock, C. A., Thomas, J. L., Starkweather, S. M., von Salzen, K., Stohl, A., Sharma, S., Lund, M. T., Flanner, M.G., Petäjä, T., Tanimoto, H., Gamble, J., Dibb, J. E., Melamed, M., Johnson, N., Fidel, M., Tynkkynen, V. -P., Baklanov, A., Eckhardt, S., Monks, S. A., Browse, J., Bozem, H.: Arctic air pollution: Challenges and opportunities for the next decade, Elementa: Science of the Anthropocene, 4, 104, https://doi.org/10.12952/journal.elementa.000104, 2016.

Aubinet, M., Vesala, T., Papale, D., et al.: Eddy Covariance. A Practical Guide to Measurement and Data Analysis, Springer Atmospheric Sciences, https://doi.org/10.1007/978-94-007-2351-1, 2012.

Bao, T., Xu, X., Jia, G., Billesbach, D. P., and Sullivan, R. C.: Much stronger tundra methane emissions during autumn freeze than spring thaw, Global Change Biol., 27, 376–387, https://doi.org/10.1111/gcb.15421, 2021.

https://doi.org/10.5194/egusphere-2024-1440
Preprint. Discussion started: 23 May 2024


Bintanja, R., and Van der Linden, E. C.: The changing seasonal climate in the Arctic, Sci Rep-UK, 3, 1556, https://doi.org/10.1038/srep01556, 2013.

Burba, G., McDermitt, D. K., Grelle, A., Anderson, D., and Xu, L.: Addressing the influence of instrument surface heat exchange on the measurements of $CO_2$ flux from open-path gas analyzers, Global Change Biol., 14, 1854–1876, https://doi.org/10.1111/j.1365-2486.2008.01606.x, 2008.

Cahoon, S. M. P., Sullivan, P. F., Post, E., and Welker, J. M.: Large herbivores limit $CO_2$ uptake and suppress carbon cycle responses to warming in West Greenland, Global Change Biol., 2, 469–479, https://doi.org/10.1111/j.1365-2486.2011.02528.x, 2012.

Christiansen, J. R., Romero, A. J. B., Jørgensen, N. O. G., Glaring, M. A., Jørgensen, C. J., Berg, L. K., and Elberling, B.: Methane fluxes and the functional groups of methanotrophs and methanogens in a young Arctic landscape on Disko Island, West Greenland, Biogeochemistry 122, 15–33, https://doi.org/10.1007/s10533-014-0026-7, 2015.

Cicerone, R. J., and Oremland, R. S.: Biogeochemical aspects of atmospheric methane, Global Biogeochem. Cy. 2, 299–327, https://doi.org/10.1029/GB002i004p00299, 1988.

Curry, C.: Modelling the soil consumption of atmospheric methane at the global scale, Global Biogeochem. Cy., 21, GB4012, https://doi.org/10.1029/2006GB002818, 2007.

Dean, J. F., Meisel, O. H., Rosco, M., Belelli Marchesini, L., Garnett, M. H., Lenderink, H., Van Logtestijn, R., Borges, A. V., Bouillon, S., Lambert, T., Röckmann, T., Maximov, T., Petrov, R., Karsanaev, S., Aerts, R., van Huissteden, J., Vonk, J. E., and Dolman, A. J.: East Siberian Arctic inland waters emit mostly contemporary carbon, Nat. Commun., 11, 1627. https://doi.org/10.1038/s41467-020-15511-6, 2020.

Dean, J. F., Van der Velde, Y., Garnett, M. H., Dinsmore, K. J., Baxter, R., Lessels, J. S., Smith, P., Street, L. E., Subke, J.-A., Tetzlaff, D., Washbourne, D., Wookey, D. A., and Billett, M. F.: Abundant pre-industrial carbon detected in Canadian Arctic headwaters: implications for the permafrost carbon feedback, Environ. Res. Lett., 13, 034024, https://doi.org/10.1088/1748-9326/aaa1fe, 2018.

D'Imperio, L., Nielsen, C. S., Westergaard-Nielsen, A., Michelsen, A., and Elberling, B.: Methane oxidation in contrasting soil types: responses to experimental warming with implication for landscape-integrated $CH_4$ budget, Global Change Biol. 23, 966–976, https://doi.org/10.1111/gcb.13400, 2017.

Donateo, A., Famulari, D., Giovannelli, D., Mariani, A., Mazzola, M., Decesari, S., Pappaccogli, G.: Observations of methane net sinks in the Arctic tundra – Data, Italian Arctic Data Center (IADC), https://doi.org/10.48230/DSET.2024.0001, 2024.

Donateo, A., Pappaccogli, G., Famulari, D., Mazzola, M., Scoto, F., and Decesari, S.: Characterization of size-segregated particles turbulent flux and deposition velocity by eddy correlation method at an Arctic site, Atmos. Chem. Phys., 23, 7425–7445, https://doi.org/10.5194/acp-23-7425-2023, 2023.

Dyukarev, E.: Comparison of Artificial Neural Network and Regression Models for Filling Temporal Gaps of Meteorological Variables Time Series, Appl. Sci. 13, 2646, https://doi.org/10.3390/app13042646, 2023.

Emmerton, C. A., St Louis, V. L., Lehnherr, I., Graydon, J. A., Kirk, J. L., and Rondeau, K. J.: The importance of freshwater systems to the net atmospheric exchange of carbon dioxide and methane with a rapidly changing high Arctic watershed, Biogeosciences, 13, 5849–5863, https://doi.org/10.5194/bg-13-5849-2016, 2016.

https://doi.org/10.5194/egusphere-2024-1440
Preprint. Discussion started: 23 May 2024


Emmerton, C. A., St Louis, V. L., Lehnherr, I., Humphreys, E. R., Rydz, E., and Kosolofski, H. R.: The net exchange of methane with high Arctic landscapes during the summer growing season, Biogeosciences, 11, 3095–3106, https://doi.org/10.5194/bg-11-3095-2014, 2014.

Finkelstein, P. L., and Sims, P. F.: Sampling error in eddy correlation flux measurements, J. Geophys. Res-Atmos., 106, 3503–3509, https://doi.org/10.1029/2000JD900731, 2001.

Gash, J. H. C., and Culf, A. D.: Applying a linear detrend to eddy correlation data in real time, Bound-Lay. Meteorol., 79(3), 301 – 306, https://doi.org/10.1007/BF00119443, 1996.

Greening, C., and Grinter, R.: Microbial oxidation of atmospheric trace gases, Nat. Rev. Microbiol., 20, 513, https://doi.org/10.1038/s41579-022-00724-x, 2022.

Guerrero-Cruz, S., Vaksmaa, A., Horn, M. A., Niemann, H., Pijuan, M., and Ho, A.: Methanotrophs: Discoveries, Environmental Relevance, and a Perspective on Current and Future Applications, Front. Microbiol. 12:678057, https://doi.org/10.3389/fmicb.2021.678057, 2021.

Hodson, A. J., Nowak, A., Redeker, K. R., Holmlund, E. S., Christiansen, H. H., and Turchyn, A. V.: Seasonal dynamics of methane and carbon dioxide evasion from an open system pingo: Lagoon Pingo, Svalbard, Front. Earth Sci. 7:30, https://doi.org/10.3389/feart.2019.00030, 2019.

Horst, T. W., and Lenschow, D. H.: Attenuation of scalar fluxes measured with spatially-displaced sensors, Bound-Lay. Meteorol., 130, 275-300, https://doi.org/10.1007/s10546-008-9348-0, 2009.

Howarth, R. W., Santoro, R., and Ingraffea, A.: Methane and the greenhouse gas footprint of natural gas from shale formations, Climatic Change, https://doi.org/10.1007/s10584-011-0061-5, 2011.

Hugelius, G., Strauss, J., Zubrzycki, S., Harden, J. W., Schuur, E. A. G., Ping, C.-L., Schirrmeister, L., Grosse, G., Michaelson, G. J., Koven, C. D., O'Donnell, J. A., Elberling, B., Mishra, U., Camill, P., Yu, Z., Palmtag, J., and Kuhry, P.: Estimated stocks of circumpolar permafrost carbon with quantified uncertainty ranges and identified data gaps, Biogeosciences, 11, 6573–6593, https://doi.org/10.5194/bg-11-6573-2014, 2014.

Kim, Y., Johnson, M. S., Knox, S. H., Black, T. A., Dalmagro, H. J., Kang, M., Kim, J., and Baldocchi, D.: Gap-filling Approaches for Eddy Covariance Methane Fluxes: A Comparison of Three Machine Learning Algorithms and a Traditional Method with Principal Component Analysis, Global Change Biol., 26, 1499–1518, https://doi.org/10.1111/gcb.14845, 2020.

Kleber, G. E., Hodson, A. J., Magerl, L., Mannerfelt, E. S., Bradbury, H. J., Zhu, Y., Trimmer, M., and Turchyn, A. V.: Groundwater springs formed during glacial retreat are a large source of methane in the high Arctic, Nat. Geosci., 16, 597–604, https://doi.org/10.1038/s41561-023-01210-6, 2023.

Kljun, N., Calanca, P., Rotach, M. W., and Schmid, H. P.: A simple two-dimensional parameterisation for Flux Footprint Prediction (FFP), Geosci. Model Dev., 8, 3695–3713, https://doi.org/10.5194/gmd-8-3695-2015, 2015.

Knoblauch, C., Beer, C., Liebner, S., Grigoriev, M. N., and Pfeiffer, E.: Methane production as key to the greenhouse gas budget of thawing permafrost, Nature Clim. Change, 8, 309–312, https://doi.org/10.1038/s41558-018-0095-z, 2018.

Knox, S. H., Bansal, S., McNicol, G., Schafer, K., Sturtevant, C., Ueyama, M., Valach, A. C., Baldocchi, D., Delwiche, K., Desai, A. R., Euskirchen, E., Liu, J., Lohila, A., Malhotra, A., Melling, L., Riley, W., Runkle, B. R. K., Turner, J., Vargas, R., Zhu, Q., Alto, T., Chouinard, E., Goeckede, M., Melton, J. R., Sonnentag, O., Vesala, T., Ward, E., Zhang, Z., Feron, S.,

https://doi.org/10.5194/egusphere-2024-1440
Preprint. Discussion started: 23 May 2024


Ouyang, Z., Alekseychik, P., Aurela, M., Bohrer, G., Campbell, D. I., Chen, J., Chu, H., Dalmagro, H. J., Goodrich, J. P., Gottschalk, P., Hirano, T., Iwata, K., Jurasinski, G., Kang, M., Koebsch, F., Mammarella, I., Nilsson, M. B., Ono, K., Peichl, M., Peltola, O., Ryu, Y., Sachs, T., Sakabe, A., Sparks, J. P., Tuittila, E., Vourlitis, G. L., Wong, G. X., Windham-Myers, L., Poulter, B., and Jackson, R. B.: Identifying dominant environmental predictors of freshwater wetland methane fluxes across diurnal to seasonal time scales, Global Change Biol., 27, 3582–3604, https://doi.org/10.1111/gcb.15661, 2021.

Kral, S. T., Sjöblom, A., and Nygård, T.: Observations of summer turbulent surface fluxes in a High Arctic fjord, Q. J. Roy. Meteorol. Soc., 140: 666–675, https://doi.org/10.1002/qj.2167, 2014.

Juncher Jørgensen, C., Lund Johansen, K. M.,Westergaard-Nielsen, A., and Elberling, B.: Net regional methane sink in High Arctic soils of northeast Greenland, Nat. Geosci., 8, 20–23, https://doi.org/10.1038/ngeo2305, 2015.

Ishizawa, M., Chan, D., Worthy, D., Chan, E., Vogel, F., and Maksyutov, S.: Analysis of atmospheric $CH_4$ in Canadian Arctic and estimation of the regional $CH_4$ fluxes, Atmos. Chem. Phys., 19, 4637–4658, https://doi.org/10.5194/acp-19-4637-2019, 2023.

Yun, J., Yang, Y., Zhou, X., Lee, J., Choi, J., Kim, M., Gyeong, H., Laffly, D., and Kang, D.: Effects of deglaciation on the succession of methanotrophic communities in inland and tidewater glaciers in the high Arctic, Svalbard, Catena, 231.107267, https://doi.org/10.1016/j.catena.2023.107267, 2023.

Lafleur, P. M., and Humphreys, E. R.: Spring warming and carbon dioxide exchange over low Arctic tundra in central Canada, Global Change Biol., 14, 740–756, https://doi.org/10.1111/j.1365-2486.2007.01529.x, 2007.

Lara, M. J., Nitze, I., Grosse, G., Martin, P., and McGuire, A. D.: Reduced arctic tundra productivity linked with landform and climate change interactions, Sci. Rep. 8, 2345, https://doi.org/10.1038/s41598-018-20692-8, 2018.

Law, K. S., Stohl, A., Quinn, P. K., Brock, C. A., Burkhart, J. F., Paris, J.-D., Ancellet, G., Singh, H. B., Roiger, A., Schlager, H., Dibb, J., Jacob, D. J., Arnold, S. R., Pelon, J., and Thomas, J. L.: Arctic air pollution: New insights from POLARCAT-IPY, B. Am. Meteorol. Soc., 95(12), 1873–1895, https://doi.org/10.1175/bams-d-13-00017.1, 2014.

Lindroth, A., Pirk, N., Jónsdóttir, I. S., Stiegler, C., Klemedtsson, L., and Nilsson, M. B.: $CO_2$ and $CH_4$ exchanges between moist moss tundra and atmosphere on Kapp Linné, Svalbard, Biogeosciences, 19, 3921–3934, https://doi.org/10.5194/bg-19-3921-2022, 2022.

Lloyd, C. R., Harding, R. J., Friborg, T., and Aurela, R.: Surface fluxes of heat and water vapour from sites in the European Arctic, Theor. Appl. Climatol., 70, 19–33, https://doi.org/10.1007/s007040170003, 2001.

Lüers, J., Westermann, S., Piel, K., and Boike, J.: Annual $CO_2$ budget and seasonal $CO_2$ exchange signals at a high Arctic permafrost site on Spitsbergen, Svalbard archipelago, Biogeosciences, 11, 6307–6322, https://doi.org/10.5194/bg-11-6307-2014, 2014.

Lucas, E. W. M., de Sousa, F. de A. S., dos Santos Silva, F. D., Lins da Rocha Jr, R., Cavalcante Pinto, D. D., and de Paulo Rodrigues da Silva, V.: Trends in climate extreme indices assessed in the Xingu river basin - Brazilian Amazon, Weather and Climate Extremes, 31, 100306, https://doi.org/10.1016/j.wace.2021.100306, 2021.

Magnani, M., Baneschi, I., Giamberini, M., Raco, M., and Provenzale, A.: Microscale drivers of summer $CO_2$ fluxes in the Svalbard High Arctic tundra, Sci. Rep., 12:763, https://doi.org/doi.org/10.1038/s41598-021-04728-0, 2022.

Massmann, W. J.: Reply to comment by Rannik on “A simple method for estimating frequency response corrections for eddy covariance systems”, Agr. For. Meteor., 107, 247–251, https://doi.org/10.1016/S0168-1923(00)00237-9, 2001.

https://doi.org/10.5194/egusphere-2024-1440
Preprint. Discussion started: 23 May 2024


Massmann, W. J.: A simple method for estimating frequency response corrections for eddy covariance systems, Agr. For. Meteor., 104, 3, 185-198, https://doi.org/10.1016/S0168-1923(00)00164-7, 2000.

Mastepanov, M., Sigsgaard, C., Tagesson, T., Ström, L., Tamstorf, M. P., Lund, M., and Christensen, T. R.: Revisiting factors controlling methane emissions from high-Arctic tundra, Biogeosciences, 10, 5139–5158, https://doi.org/10.5194/bg-10-5139-2013, 2013.

Mastepanov, M., Sigsgaard, C., Dlugokencky, E. J., Houweling, S., Strom L., Tamstorf, M. P., and Christensen, T. R.: Large tundra methane burst during onset of freezing, Nature, 456, 628–631, https://doi.org/10.1038/nature07464, 2008.

Mauder, M., Cuntz, M., Drüe, C., Graf, A., Rebmann, C., Schmid, H. P., Schmidt, M., and Steinbrecher, R.: A strategy for quality and uncertainty assessment of long-term eddy-covariance measurements, Agr. For. Meteor., 169, 122–135, https://doi.org/10.1016/j.agrformet.2012.09.006, 2013.

Mauder, M., and Foken, T.: Documentation and instruction manual of the eddy covariance software package TK2, Arbeitsergebnisse, Universitat at Bayreuth, Abt. Mikrometeorologie 26, 45, 2004.

Mazzola, M., Viola, A. P., Choi, T., and Tampieri, F.: Characterization of Turbulence in the Neutral and Stable Surface Layer at Jang Bogo Station, Antarctica, Atmosphere, 12, 1095, https://doi.org/10.3390/atmos12091095, 2021.

Mazzola, M., Tampieri, F., Viola, A. P., Lanconelli, C., and Choi, T.: Stable boundary layer vertical scales in the Arctic: observations and analyses at Ny-Ålesund, Svalbard, Q. J. Roy. Meteor. Soc., 142: 1250–1258, https://doi.org/10.1002/qj.2727, 2016.

McDermitt, D., Burba, G., Xu, L., Anderson, T., Komissarov, A., Riensche, B., Schedlbauer, J., Starr, G., Zona, D., Oechel, W., Oberbauer, S., and Hastings, S.: A new low-power, open-path instrument for measuring methane flux by eddy covariance, Appl. Phys. B 102, 391–405, https://doi.org/10.1007/s00340-010-4307-0, 2011.

Moncrieff, J., Clement, R., Finnigan, J., and Meyers, T.: Averaging, detrending, and filtering of eddy covariance time series, Handbook of Micrometeorology. pp. 7 – 31, https://doi.org/10.1007/1-4020-2265-4_2, 2004.

Myhre, G., Shindell, D., Bréon, F.-M., Collins, W., Fuglestvedt, J., Huang, J., Koch, D., Lamarque, J.-F., Lee, D., Mendoza, B., Nakajima, T., Robock, A., Stephens, G., Takemura, T., and Zhang, H.: Anthropogenic and natural radiative forcing. In: Stocker, T.F., Qin, D., Plattner, G.-K., Tignor, M., Allen, S.K., Boschung, J., Nauels, A., Xia, Y., Bex, V., Midgley, P.M. (Eds.), Climate Change (2013). The Physical Science Basis. Contribution of Working Group I to the Fifth Assessment Report of the Intergovernmental Panel on Climate Change. Cambridge University Press, Cambridge, United Kingdon and New York, NY, USA, 2013.

Nakai, T., Van der Molen, M., Gash, J., and Kodama, Y.: Correction of sonic anemometer angle of attack errors, Agr. For. Meteor., 136(1), 19–30, https://doi.org/10.1016/j.agrformet.2006.01.006, 2006.

Oh, Y., Zhuang, Q., Liu, L., Welp, L. R., Lau, M. C. Y., Onstott, T. C., Medvigy, D., Bruhwiler, L., Dlugokencky, E. J., Hugelius, G., D'Imperio, L., and Elberling, B.: Reduced net methane emissions due to microbial methane oxidation in a warmer Arctic, Nature Clim. Change, vol. 10, 317–321, https://doi.org/10.1038/s41558-020-0734-z, 2020.

Ohtsuka, T., Adachi, M., Uchida, M., and Nakatsubo, T.: Relationships between vegetation types and soil properties along a topographical gradient on the northern coast of the Brøgger Peninsula, Svalbard, Polar Biosci., 19, 63–72, oai:nipr.repo.nii.ac.jp:00006240, 2006.

https://doi.org/10.5194/egusphere-2024-1440
Preprint. Discussion started: 23 May 2024


Papale, D., Reichstein, M., Aubinet, M., Canfora, E., Bernhofer, C., Kutsch, W., Longdoz, B., Rambal, S., Valentini, R., Vesala, T., and Yakir, D.: Towards a standardized processing of Net Ecosystem Exchange measured with eddy covariance technique: algorithms and uncertainty estimation, Biogeosciences, 3(4), 571-583, https://doi.org/10.5194/bg-3-571-2006, 2006.

Pedregosa, F., Varoquaux, G., Gramfort, A., Michel, V., Thirion, B., Grisel, O., Blondel, M., Prettenhofer, P., Weiss, R., Dubourg, V., Vanderplas, J., Passos, A., Cournapeau, D., Brucher, M., Perrot, M., and Duchesnay, E.: Scikit-learn: Machine Learning in Python, J. Mach. Learn. Res., 12, 2825–2830, https://doi.org/10.5555/1953048.2078195, 2011.

Pirk, N., Tamstorf, M. P., Lund, M., Mastepanov, M., Pedersen, S. H., Mylius, M. R., Parmentier, F.-J., Christiansen, H. H., and Christensen, T. R.: Snowpack fluxes of methane and carbon dioxide from high Arctic tundra, J. Geophys. Res.-Biogeo., 121(11), 2886–2900, https://doi.org/10.1002/2016j g003486, 2016.

Pirk, N., Santos, T., Gustafson, C., Johansson, A. J., Tufvesson, F., Parmentier, F.-J., Mastepanov, M., and Christensen, T. R.: Methane emission bursts from permafrost environments during autumn freeze-in: New insights from ground-penetrating radar, Geophys. Res. Lett., 42(16), 6732–6738, https://doi.org/10.1002/2015G L065034, 2015.

Reichstein, M., Falge, E., Baldocchi, D., Papale, D., Aubinet, M., Berbigier, P., Bernhofer, C., Buchmann, N., Gilmanov, T., Granier, A., Grünwald, T., Havránková, K., Ilvesniemi, H., Janous, D., Knohl, A., Laurila, T., Lohila, A., Loustau, D., Matteucci, G., Meyers, T., Miglietta, F., Ourcival, J.-M., Pumpanen, J., Rambal, S., Rotenberg, E., Sanz, M., Tenhunen, J., Seufert, G., Vaccari, F., Vesala, T., Yakir, D., and Valentini, R.: On the separation of net ecosystem exchange into assimilation and ecosystem respiration: review and improved algorithm, Global Change Biol., 11, 1424–1439, https://doi.org/10.1111/j.1365-2486.2005.001002.x, 2005.

Reay, D., Hewitt, C. N., Smith, K., and Grace, J.: Greenhouse Gas Sinks, CABI, Oxfordshire, ISBN 978-1-84593-189-6, 2007.

Sachs, T., Wille, C., Boike, J., and Kutzbach, L.: Environmental controls on ecosystem-scale $CH_4$ emission from polygonal tundra in the Lena River Delta, Siberia, J. Geophys. Res.-Biogeo.,113, G00A03, https://doi.org/10.1029/2007JG000505, 2008.

Sand, M., Berntsen, T. K., von Salzen, K., Flanner, M. G., Langner, J., and Victor, D. G.: Response of Arctic temperature to changes in emissions of short-lived climate forcers, Nature Clim. Change, 6(3), 286–289, https://doi.org/10.1038/nclimate2880, 2015.

Serreze, M. C., and Barry, R. G.: Processes and impacts of Arctic amplification: A research synthesis, Global Planet. Change, 77, 85–96, https://doi.org/10.1016/j.gloplacha.2011.03.004, 2011.

Serrano-Silva, N., Sarria-Guzman, Y., Dendooven, L., and Luna-Guido, M.: Methanogenesis and methanotrophy in soil: a review, Pedosphere 24, 291–307, https://doi.org/10.1016/S1002-0160(14)60016-3, 2014.

Schmale, J., Zieger, P., and Ekman, A. M. L.: Aerosols in current and future Arctic climate, Nat. Clim. Change, 11, 95–105, https://doi.org/10.1038/s41558-020-00969-5, 2021.

Sievers, J., Sørensen, L. L., Papakyriakou, T., Else, B., Sejr, M. K., Haubjerg Søgaard, D., Barber, D., and Rysgaard, S.: Winter observations of $CO_2$ exchange between sea ice and the atmosphere in a coastal fjord environment, Cryosphere, 9, 1701–1713, https://doi.org/:10.5194/tc-9-1701-2015, 2015.

Stjern, C. W., Lund, M. T., Samset, B. H., Myhre, G., Forster, P. M., Andrews, T., et al.: Arctic amplification response to individual climate drivers, J. Geophys. Res.-Atmos., 124, 6698–6717, https://doi.org/10.1029/2018JD029726, 2019.

https://doi.org/10.5194/egusphere-2024-1440
Preprint. Discussion started: 23 May 2024


Stull, R. B.: An introduction to boundary layer meteorology, Kluwer Academic Publishers, Dordrecht, ISBN 978-90-277-2769-5, 1998.

Tan, Z., Zhuang, Q., Henze, D. K., Frankenberg, C., Dlugokencky, E., Sweeney, C., Turner, A. J., Sasakawa, M., and Machida, T.: Inverse modeling of pan-Arctic methane emissions at high spatial resolution: what can we learn from assimilating satellite retrievals and using different process-based wetland and lake biogeochemical models?, Atmos. Chem. Phys., 16, 12649–12666, https://doi.org/10.5194/acp-16-12649-2016, 2016.

Taylor, M. A., Celis, G., Ledman, J. D., Bracho, R., and Schuur, E. A. G.: Methane efflux measured by eddy covariance in Alaskan upland tundra undergoing permafrost degradation, J. Geophys. Res.-Biogeo., 123(9), 2695–2710, https://doi.org/10.1029/2018J G004444, 2018.

Treat, C. C., Virkkala, A.-M., Burke, E., Bruhwiler, L., Chatterjee, A., Fisher, J. B., et al.: Permafrost carbon: Progress on understanding stocks and fluxes across northern terrestrial ecosystems, J. Geophys. Res.-Biogeo., 129, e2023JG007638, https://doi.org/10.1029/2023JG007638, 2024.

Treat, C.C., Jones, M. C., Camill, P., Gallego-Sala, A., Garneau, M., Harden, J. W., Hugelius, G., Klein, E. S., Kokfelt, U., Kuhry, P., Loisel, J., Mathijssen, P. J. H., O'Donnell, J. A., Oksanen, P. O., Ronkainen, T. M., Sannel, A. B. K., Talbot, J., Tarnocai, C., and Väliranta, M.: Effects of permafrost aggradation on peat properties as determined from a pan-Arctic synthesis of plant macrofossils, J. Geophys. Res-Biogeo.,121,78–94, https://doi.org/10.1002/2015JG003061, 2016.

Vickers, D., and Mahrt, L.: Quality control and flux sampling problems for tower and aircraft data, J. Atmos. Ocean. Tech., 14(3), 512–526, https://doi.org/10.1175/1520-0426(1997)014, 1997.

Voigt, C., Virkkala, A.-M., Gosselin, J. H., Bennett, K. A., Black, T. A., Detto, M., Chevrier-Dion, C., Guggenberger, G., Hashmi, W., Kohl, L., Kou, D., Marquis, C., Marsh, P., Marushchak, M. E., Nesic, Z., Nykänen, H., Saarela, T., Sauheitl, L., Walker, B., Weiss, N., Wilcox, E. J., and Sonnentag, O.: Arctic soil methane sink increases with drier conditions and higher ecosystem respiration, Nature Clim. Change, 13, 1095–1104, https://doi.org/10.1038/s41558-023-01785-3, 2023.

Uchida, M., Kishimoto, A., Muraoka, H., Nakatsubo, T., Kanda, H., and Koizumi, H.: Seasonal shift in factors controlling net ecosystem production in a high Arctic terrestrial ecosystem, J. Plant Res., 123, 79–85, 2009.

Wagner, I., Hung, J. K. Y., Neil, A., and Scott, N. A.: Net greenhouse gas fluxes from three High Arctic plant communities along a moisture gradient, Arct. Sci., 5, 185–201, https://doi.org/10.1139/as-2018-0018, 2019.

Wang, J. M., Murphy, J. G., Geddes, J. A., Winsborough, C. L., Basiliko, N., and Thomas, S. C.: Methane fluxes measured by eddy covariance and static chamber techniques at a temperate forest in central Ontario, Canada, Biogeosciences, 10, 4371–4382, https://doi.org/10.5194/bg-10-4371, 2013.

Wartiainen, I., Hestnes, A. G., McDonald, I. R., and Svenning, M. M.: Methylocystis rosea sp. nov., a novel methanotrophic bacterium from Arctic wetland soil, Svalbard, Norway (78° N), Int. J. Syst. Evol. Mic., 56, 541–547, https://doi.org/10.1099/ijs.0.63912-0, 2006a.

Wartiainen, I., Hestnes, A. G., McDonald, I. R., and Svenning, M. M.: Methylobacter tundripaludum sp. nov., a methane-oxidizing bacterium from Arctic wetland soil on the Svalbard islands, Norway (78° N), Int. J. Syst. Evol. Micr., 56, 109–113, https://doi.org/10.1099/ijs.0.63728-0, 2006b.

Webb, E. K., Pearman, G. I., and Leuning, R.: Correction of the flux measurements for density effects due to heat and water vapour transfer, Q. J. Roy. Meteor. Soc., 106, 85–100, https://doi.org/10.1002/qj.49710644707, 1980.

https://doi.org/10.5194/egusphere-2024-1440
Preprint. Discussion started: 23 May 2024


Wilczak, J. M., Oncley, S. P., and Stage, S. A.: Sonic anemometer tilt correction algorithms, Bound-Lay. Meteorol., 99, 127–150, https://doi.org/10.1023/A:1018966204465, 2001.

Wille, C., Kutzbach, L., Sachs, T., Wagner, D., and Pfeiffer, E.-M.: Methane emission from Siberian arctic polygonal tundra: eddy covariance measurements and modelling, Global Change Biol., 14, 1395–1408, https://doi.org/10.1038/s41558-022-01512-4, 2008.

Winther, J.-G., Bruland, O., Sand, K., Gerland, S., Marechal, D., Ivanov, B., Glowacki, P., and König, M.: Snow research in Svalbard - an overview, Polar Research, 22, 125–144, https://doi.org/10.1111/j.1751-8369.2003.tb00103.x, 2003.

Zemmelink, H. J., Delille, B., Tison, J. L., Hintsa, E. J., Houghton, L., and Dacey, J. W. H.: $CO_2$ deposition over the multi-year ice of the western Weddell Sea, Geophys. Res. Lett., 33, L13606, https://doi.org/10.1029/2006gl026320, 2006.

Zona, D., Lafleur, P. M., Hufkens, K., Gioli, B., Bailey, B., Burba, G., Euskirchen, E. S., Watts, J. D., Arndt, K. A., Farina, M., Kimball, J. S., Heimann, M., Göckede, M., Pallandt, M., Christensen, T. R., Mastepanov, M., López-Blanco, E., Dolman, A. J., Commane, R. … Oechel, W. C.: Pan-Arctic soil moisture control on tundra carbon sequestration and plant productivity, Global Change Biol., 29, 1267–1281, https//doi.org/10.1111/gcb.16487, 2022.

Zona, D., Gioli, B., Commane, R., Lindaas, J., Wofsy, S. C., Miller, C. E., Dinardo, S. J., Dengel, S., Sweeney, C., Karion, A., Chang, R.-W., Henderson, J. M., Murphy, P. C., Goodrich, J. P., Moreaux, V., Liljedahl, A., Watts, J. D., Kimball, J. S., Lipson, D. A., and Oechel, W. C.: Cold season emissions dominate the Arctic tundra methane budget, P. Natl. Acad. Sci. USA, 113(1), 40–45, https://doi.org/10.1073/pnas.15160 17113, 2016.